MULTI-FREQUENCY STUDY OF PULSAR B1929+10

A thesis submitted towards partial fulfilment of
BS-MS Dual Degree Programme

by

KARISHMA BANSAL

under the guidance of

AVINASH A DESHPANDE

RAMAN RESEARCH INSTITUTE, BENGALURU

INDIAN INSTITUTE OF SCIENCE EDUCATION AND
RESEARCH PUNE

Acknowledgements

Abstract

Time sequences of signals received from PSR 1929+10 have been recorded using RRI-MBR receiver. This receiver facilitates observations in ten frequency bands simultaneously. These voltage time sequences are further processed to obtain spectral information. Average profiles for all the bands are obtained by folding the time sequences and averaging the weighted channels. We had aimed to study âĂİnotchesâĂİ but due to inadequate signalto noise ratio , it does not appear possible. Instead, we have studied the evolution of the component separation.

However, two undesirable features in the data of our one of the best bands. First is an effect of gain compression, which occurs due to even a slight deviation of amplifier response linearity, encountered when input signal is high. A correction technique exploiting the dispersed nature of pulsar sig- nal has been developed successfully.

The second undesirable feature was in form of a strange RFI signal which was narrowed band but periodic within each of its episode.

We also explored the possibility of studying its polarization features across the multi bands with an eventual aim of estimating the possible shifts between profile peak and points of inflection in the position angle sweep. These shifts are expected to provide estimates of emission heights at respective frequencies. We discuss our multi-frequency observations of this pulsar, the analysis details and implications of our results.

Contents

Chapter 1

Introduction

1.1   Pulsar:

Pulsars are rotating magnetized neutron stars which emit pulse radiation along narrow beam. Though Pulsars are known as pulsating stars, the emission is actually continuous. The reason that the observed emission appears pulsed is due to misalignment between the rotation and the magnetic axis. The emission is observed only when the pulsar beam points towards earth during rotation. They were discovered by Jocelyn Bell and Anthony Hewish in 1967. Jocelyn observed a series of periodic pulses with varying amplitudes. At first it was thought to be terrestrial as the spacing between the pulses was highly regular. But later it was established that these were not man-made and the unknown object was named as *Pulsar*. PSR 1919+21 is the first discovered pulsar.

1.2   Formation:

Exhaustion of nuclear fuel in normal star (8-20 $M_\odot$) leads to collapse under gravity from its stable state to a condensed state. At the Chandrasekhar limit core collapses, and electron degeneracy pressure is not able to balance gravitational collapse. As a result the density of the core increases. The further collapse is prevented by the degeneracy pressure of neutrons and releases gravitational energy which throws away the outer layers of the star leads to the supernova explosion and formation of a neutron star at the center. Neutron stars are expected to have mass in range of 1.3 to 2.3 $M_\odot$.
Neutron stars are very dense sand have density same as nuclear density($\sim$

10^{15} gm/cc). They spin very fast and have a tiny radius of only about 10 km and possess large magnetic fields (10^{12} Gauss) which are primarily dipolar.

1.3   Distance:

Pulsars are at a large distance (few hundreds of thousands light years) from us. The nearest pulsar is at 300 light years. The distance to pulsars is usually estimated using Dispersion Measure(DM) and rotation measure(RM).

$$DM = \int_0^D n_e dl \tag{1.1}$$

$$RM = \int_0^D n_e B_{||} dl \tag{1.2}$$

Parallax and proper motion are also used to determine distances but only for nearby pulsars.
H1 line of emission and absorption by the clouds is another tool which can also be used to obtain the distance. As, emission from the clouds behind the pulsar will overestimate the distance and absorption by clouds in front of the pulsar will underestimate the distance. Thus by combining both the estimation correct distance is obtained.

1.4   Period:

Periods of pulsars are remarkably stable and they are even called as perfect clocks. These ranges from 1.56 millisecond to 8.5 seconds. The spinning rate of pulsar decreases due to loss of rotational energy via magnetic dipole radiation. The rate of period increment can also be estimated by dP/dt, typically of the order of 10^{15} in units of sec/sec. Though the rate of slowing down is very small it can be measured precisely. The rate of energy loss is given as:

$$W = I\omega d\omega/dt \tag{1.3}$$

where, W is energy loss rate, I is moment of inertia, ω is angular frequency
Using the above estimated $\dot{P}$, the surface magnetic field is estimated which is proportional to $P\dot{P}$

Sudden change in pulsars rotation rate is termed as *Glitches*. This also leads to change in pulsar period.

1.5 Observed Features:

1.5.1 Profile:

Integrated pulse is obtained by averaging thousands of individual pulses. Each pulsar has a unique and identifiable pulse profile which remains stable in shape. These are generally confined to a small portion (< 10) of the pulse period.

The main pulse contains distinct number of components. Pulsar emission has been divided in two categories as core and conal emission. Core emission is believed to be originating near the magnetic field axis whereas conal emission is coming from the boundary region. Usually the main pulse is dominated by the core component at higher frequencies. These have been classified into five profile types, S_t(core single), S_d(conal single), D(double), T(triple) and M(multiple) based on number of components present in the profile ([1]). As the frequency increases the separation between the components coming from conal emission decreases. This can be attributed to radius to frequency mapping, higher frequency components are emitted close to the surface of star and lower frequency at farther away. This trend is observed due to flaring of magnetic field lines in the emission cone. As, the height of cone increases the separation between the magnetic field lines also increases.

An inter-pulse, almost halfway from the main pulse, is observed in some pulsar profiles. This could be due to two possible reasons. Either the emission from the other magnetic pole is beamed towards us, when the angle between rotation and magnetic axes $\sim 90°$, or from the same pole if it has broad emission region and the angle between rotation and magnetic axes is very small. The intensity of inter-pulse is usually 1-2% of the main pulse.

Though the integrated pulse is quite stable but individual pulses differ from each other in intensity, shape and polarization. If Subpulses have different time of arrival due to which a drift is observed. This can be attributed to the motion of *sparks* in the emission region. It has been observed that sometimes a few pulses vanish from the profile though the periodicity is maintained. This phenomena is called *Nulling*.
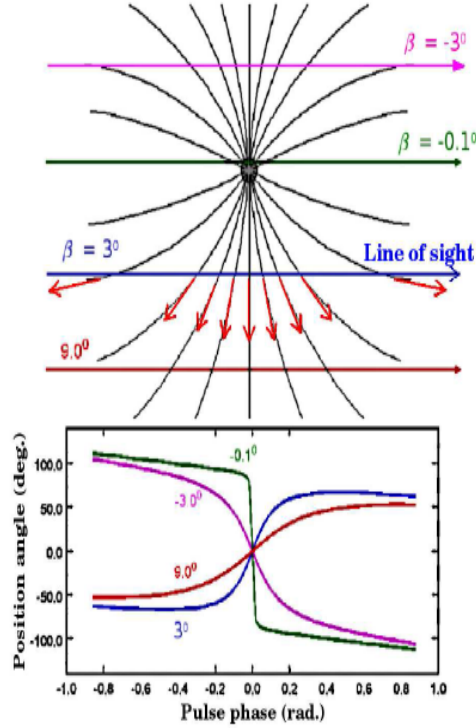
Figure 1.1: This illustrates the magnetic pole model. The black lines represent the projected magnetic field lines. Different color lines correspond to line of sight at different position. The plot shows PA profile corresponding to each PA profile.(Figure courtesy: Alice,K Harding, Frontiers of Astronomy with the World's Largest Radio Telescope meeting, 2007)

1.5.2 Polarization:

Pulsar emission is usually polarized having high degree of linear polarization. A systematic sweep of plane of polarization along the longitude is observed leading to S-shaped position angle profile. This sweep is observed due to rotation of neutron star having an inclined magnetic axis. ([2]) The position angle as a function of longitude is given by

$$\tan(\psi - \psi_0) = (\sin(\alpha)\sin(\phi - \phi_0))/(\sin(\alpha + \beta)\cos(\alpha) - \sin(\alpha)\cos(\alpha + \beta)\cos(\phi - \phi_0)) \quad (1.4)$$

where ϕ_0 is longitude of the fiducial plane, ψ_0 is position angle at ϕ_0, α is angle of inclination, *beta* is impact angle (angle made by the line of sight.) The rate of position angle swing is maximum when the line of sight is on

the magnetic axis, $\phi_0 = \psi_0$. The maximum rate is given by

$$d\psi/d\phi = \sin(\alpha)/\sin(\beta) \qquad (1.5)$$

The observed sweep profile of many pulsars is different from the above equation. There also exists two modes of polarization in a few pulsars profiles. These modes are orthogonal to each other.

1.6 Emission Mechanism:

Pulsars have primarily dipolar magnetic field. The rotation axis and the axis of magnetic field are in general at an angle with each other. Though various models have been suggested to explain the emission geometry of pulsar yet so far none of them fits the observations satisfactorily.
High brightness temperature (10^{25}-10^{30} K) of pulsar radio emission implies that pulsars do not have thermal emission not even incoherent non-thermal emission but some coherent mechanism is taking place.
The first basic and most important model by Radhakrishnan and Cooke ([2]) where in based on the polarization observations it was suggested that the emission occurs near the magnetic axis.

The plasma-filled magnetosphere in the open field region is responsible for the observed radiation This region corotates with the star till the velocity becomes comparable to the speed of light.

$$V = \Omega \times R \qquad (1.6)$$

As the distance from the pulsar increases the velocity of the corotating particles also increases. The light cylinder is defined at a radius where velocity of particles becomes equal to velocity of light, beyond which corotation ceases.
The corotating magnetosphere contains closed field lines which rotate with the pulsar. Open field lines extend beyond the light cylinder. The emission takes place only along open field lines. The region from where open field lines emerge is known as polar cap region.

The second model is Goldriech and Julian model ([3]). In this model magnetic axis is considered to be aligned with rotation axis. Their description of charge and current density in the magnetosphere remain a basis model for other as well. They divide the pulsar magnetosphere into three regions. 1. Near and wind zone. 2. Boundary zone. Near zone
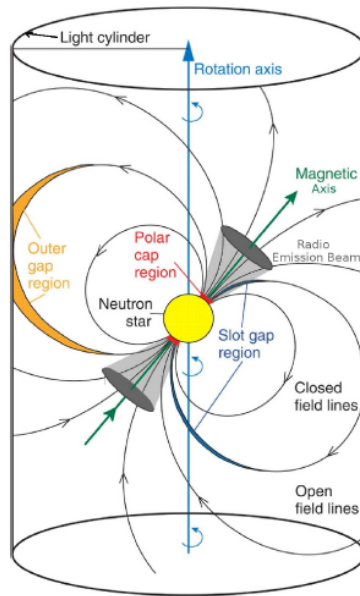
Figure 1.2: Pulsar toy model. (www.eurekalert.org)

is light cylinder zone. Wind zone is up to R/10(radius of star shell) and boundary zone beyond R/10.

Due to pulsar rotation and magnetic field, electric field is generated near the surface of pulsar. This eventually leads to a dense magnetosphere. The charged particles arrange themselves in such a way that the electric field gets canceled in most the regions. But some fraction of it survives in the polar cap region such that there is potential difference of about 10^{12} volts ([4]), between the star surface and the surrounding. Due to high potential difference no charges are found in this region and it appears like a 'vacuum gap'. If any charge enters this gap, it gets accelerate and attains relativistic energy and then emits photons. If these charged particles and photons interact with magnetic field lines and have energy greater than $2m_ec^2$, then electron-positron pair production takes place. One of the charges is sent away from the surface and other one towards the surface depending on the direction of electric field.

Once, charges going away from the surface, leave this region their motion, and of the pairs they further produce, is outward and is determined by the magnetic field lines. If the charges and photons have sufficient energy they produce a cascade of pairs of electrons and positrons. Now, primary and secondary all charges flowing out irrespective the sign of charges. Due to

9

constrain to move along the magnetic field lines, they experience acceleration. Thus, they give out curvature radiation.

1.7 Notches:

Notches are double dip W-like looking features, which have been observed in PSR B1929+10 ([5]), J0437-4715 ([6]) and B0950+08 ([7]). Since, all these pulsars are nearby, thus it enables one to observe weak emission as well. The observed features of the notches are as follows:
1. Double dip features are of same equivalent width.
2. The phase of their centroid has found to be frequency independent ([7]).
3. Rankin ([5]) have reported the separation between notches for normal pulsars to be around $10°$ and $3.3°$ for the millisecond pulsars.
4. The width and the separation between them is frequency dependent. The separation between the notches decreases with increasing frequency $\Delta \propto \nu_{obs}^{1/2}$([12]).
5. Notches have different dip level([10])
6. These features are embedded in the weak emission. In J0437-4715 it has been observed at some $70°$.These notches fall on the trailing edge of this stars very broad profile, after the bright central component. In B0950+08 ,these are near main-pulse at about $270°$, which makes it difficult to study as it may get contaminated. In B1929+10, these features have been observed at longitude $103.5°$, which is far from the main-pulse as well as from the inter-pulse. Thus, this pulsar is a good candidate to study these features.
7. These features may not be detected at some frequencies at all.
  Following models have been suggested to understand the above mentioned observations:

    1. Wright ([8]). suggested a model by considering the effects of aberration and retardation. According to this model there exists a single absorber, corrotating with the pulsar within the light cylinder. This obscuring region can exist due to locally high particle density at high energies. The narrow beam emission from pulsar provides an environment that can lead to double eclipsing by one obscuring from an extended emitting region (explains the broadness 10), and thus resulting in two notches. Though it explains the double dips and the frequency independent distance between the main pulse and the notches but still remains unable to provide reason for observed W-shape and also the evolution of separation with frequency.
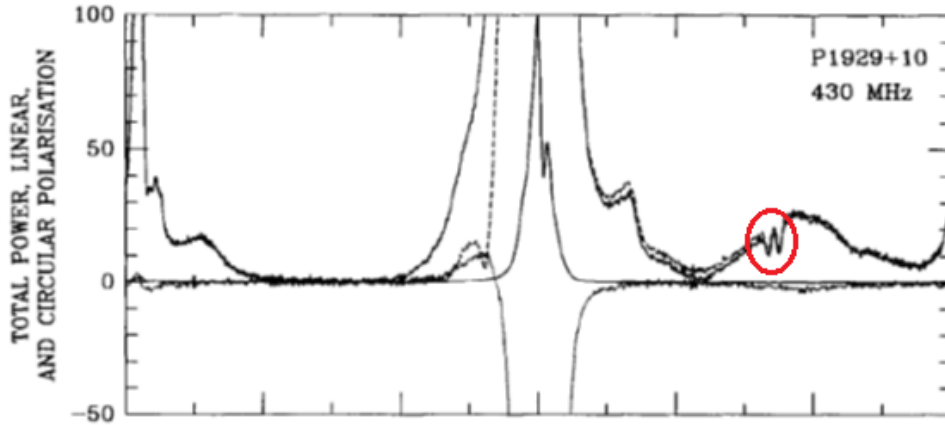
Figure 1.3: The red color circle encircles the notches.

2. Dyks et al ([9]) proposed a free maser model based on the coherent inverse Compton scattering of the parallel acceleration maser. According to this model, notches occur due to a hole in the emission region as this leads to reduction in emission. It assumes that radiation is emitted in hollow cones in the direction of the magnetic field line when electrons are accelerated parallel to their velocity a | | v. The frequency dependence of separation between the notches of the observations $\Delta \propto \nu_{obs}^{1/2}$ is consistent with this emission mechanism. It explains the symmetry and double shape of notches. This model fits perfectly at 0.82 GHz but deviates a lot at 1.42 GHz.

3. Dyks et al ([10]) proposed another model which discards the parallel beam emission mechanism and considers orthogonal mode curvature radiation. A stream of emitter moves along the magnetic field lines. Due to orthogonal mode curvature radiation there is no emission with in magnetic-line plane. The particles emit radiation in two directions thus having two emission spots. In this model, a thin opaque region of plasma above the emission region leads to formation of notches.

According to this model, the S-shaped variation in polarization position angle is observed not due to sweep across the magnetic field lines but due to the microphysical polarisation structure of the orthogonal-mode curvature pattern. The *fan-beam* formation due to curvature radiation explains various phenomena such as inter-pulse, frequency independency of the separation between the main-pulse and inter-pulse.

Our aim was to study these features present in B1929+10, but due to

poor signal to noise ratio we could not detect them.

1.8 Observations:

Raw voltages were recorded across 16MHZ bandwidth, following Nyquist sampling criterion for dual polarization in ten frequency bands, using RRI-GBT Multi-band receiver (MBR) [11]. MBR is a receiver that records data in ten discrete frequencies spanning a wide spectral range (100-1500 MHz) and two orthogonal polarization modes simultaneously. Thus, it enables one to study a source at multi-frequencies and also its polarization. This receiver has been installed on GBT, which is a 110 m single dish radio telescope.

1.9 Raw Data processing:

In blocks of 512 voltage samples in time domain are Fourier transformed to obtain 256 frequency channels. Modulus Square of complex voltages in fourier transform gives the intensity (power) spectrum. Thus, intensities along X and Y axis are obtained. The cross-correlation of X and Y is calculated to obtain stokes U and V spectra. These parameters are stored in .spec files. These files are used for further analysis.

1.10 Aim and Motivation:

B1929+10 is a well-studied pulsar. It exhibits various phenomena such as "notches" in the profile, and polarized emission across the entire longitude range, including an inter-pulse. As it is a nearby pulsar which provides us an opportunity to study even these weak radiation features. It has one of the highest and most consistent polarisations of any known pulsar and hence, it is used for polarization calibration. It exhibits two polarization modes where primary mode dominates the secondary mode. The secondary mode has been observed at around ~ 4 longitude from the centre.

Its emission geometry is still a mystery as we do not know whether the observed emission is from a single pole or two poles. The α and β obtained from the shallow PA traverse indicates single pole emission, but the profile geometry with the inter-pulse indicates α and β to be $\sim 90°$ and $\sim 0°$

respectively and hence, two-pole emission geometry.

Using the observed multi-frequency data we aim to study the radio emission across the wide range of frequencies. We also plan to study its polarization, via Faraday tomography, that will help us to understand the emission geometry.

The data analysis includes folding the data in time domain to obtain the average pulse profiles and enhance signal to noise ratio. The folded profiles across the channels are later corrected for dispersion effects caused to interstellar stellar medium. Average profiles from all the frequency bands are aligned to obtain a composite picture of spectral evolution of profiles. This enables one to study the variation in pulse shape and separation between the components with frequency.

Chapter 2

Data Analysis

2.1 How to obtain average profiles?

Radio pulses of a pulsar vary with time but the average pulse remains the same. Its stability denotes that there is a permanent underlying signature in the emission zone. B1929+10 is a short-period normal pulsar with period 0.226 seconds. Its main profile exhibits five components (observed by Rankin et al), though we have been able to see only two clear components. For band-3, we have observed an inter-pulse also.

The 'Spec' files (containing dynamic spectra, i.e. intensity as a function of frequency and time) that were obtained from the raw voltage data are further processed. By combining X and Y intensities stokes-I and stokes-Q are obtained. We fold the time sequence over the pulsar rotation period for all the Stokes parameters. Thus we obtain, for each Stokes parameter, an intensity matrix corresponding to a frequency pulse-phase plane.

2.1.1 De-dispersion

The first step is to correct for the effects of interstellar dispersion caused due to plasma present in the intervening the medium. When a signal passes through this medium, it interacts with the electrons, and due to this interaction the speed of different wavelength components changes differently, and that causes a relative delay gradient in their arrival. Dispersion occurs due to the dependence of the group velocity on the frequency of light. Due to dispersion, signals at lower frequencies arrive later than those at the higher frequencies. This delay can be corrected by suitable de-dispersion. There are two distinct de-dispersion techniques.
1. Coherent De-dispersion:

This is a pre-detection technique. The delay gradient can be viewed in terms of the differential phase change caused due to dispersion. In this technique the signal is de-convolved (using an inverse chirp function) from dispersion effects before it is passed through the detector. Long sequences of raw voltages are first Fourier transformed and then multiplied by a non-linear phase correction factor. After multiplication, inverse fourier transform is applied to obtain the de-dispersed signal. This correction is applied for whole bandwidth B, and this can potentially provide time resolution upto 1/B.

2. Incoherent De-dispersion:

This is a post-detection technique. The bandwidth is divided into many frequency channels. For each channel time delay is calculated and then later corrected individually.

The difference in times of arrival between two frequencies can be given as

$$t_d = KDM(1/f_1^2 - 1/f_2^2) \tag{2.1}$$

where,

$$DM = \int_0^D n_e dl \tag{2.2}$$

is the dispersion measure of pulsar, measured in pc/cm$^-$3. n_e is electron density present in the interstellar medium in cm^{-3} and D is physical distance in pc.

K = $4.19 * 10^6$

f_1 and f_2 are frequencies in MHz and t_d is in millisecond.

When B(Bandwidth)$<<$ f_0 then,

$$t_d = BDM(202/f_0)^3 \tag{2.3}$$

f_0 is central frequency. Even after correcting for time-delay for each channel, signal within the channels still remains dispersed.

$$t_d = BDM(202/f_0)^3/Nchn \tag{2.4}$$

i This is the smearing caused due to dispersion within each channel. This is inversely proportional to the number of channels. If the number of channels is very large then the channel width will be small, and also the smearing. Thus the de-dispersion will be more effective. But as the number of channels increases, the resolution in time domain decreases. So we need to calculate optimum number of channels in order to have less smearing and good resolution.

Time resolution can be given as:

$$t_r = Nchn/B \qquad (2.5)$$

Optimum number of channels, for which t_d equals t_r, can be given by:

$$Nchn = B\sqrt{(DM(202/f_0)^3)} \qquad (2.6)$$

Here, we have used 256 frequency channels. At frequency 327MHz, maximum smearing caused due to dispersion within the channel is 0.0468 millisec.

For this pulsar, we had aimed to study notches, which require resolution of at least 0.00125 sec, This is much larger than the smearing caused due to incoherent de-dispersion. We have used incoherent de-dispersion technique. Though coherent de-dispersion is more effective than incoherent de-dispersion, but it is computationally more expensive also.

2.1.2   DM estimation:

Dispersion measure can be calculated by measuring the relative time delay between the pulse arrivals at two frequencies. Here, it was estimated by taking a range of DM values. For each DM value, dispersion correction was done and corresponding signal to noise ratio (SNR) and Intensity square integrated across the pulse, which we call (a figure of) *merit*, was calculated for the average profile. This quantity can be shown to be a measure of compactness of a profile.

Following plots show the variation in SNR and Merit with DM:

As, we can see, that though both SNR and merit have similar DM dependence, SNR-plot shows more fluctuation. So, the DM value has been estimated from Merit-DM relation. For the actual DM value, the merit attains maxima.

These fluctuation can be attributed to fluctuation in the apparent standard deviation of noise, as the variation in pulse peak with DM is very smooth and similar to merit. We tried to investigate the reason behind these fluctuations by computing the fourier transform of noise. As their spectra (via fourier tansform) looked similar for all the DM values, a possibility of any systematic changes that could be potentially be caused by an isolated fluctuation feature (such as 50 or 100 Hz mains contamination increasing at one DM) is ruled out. Although the real reason is not clear yet, there
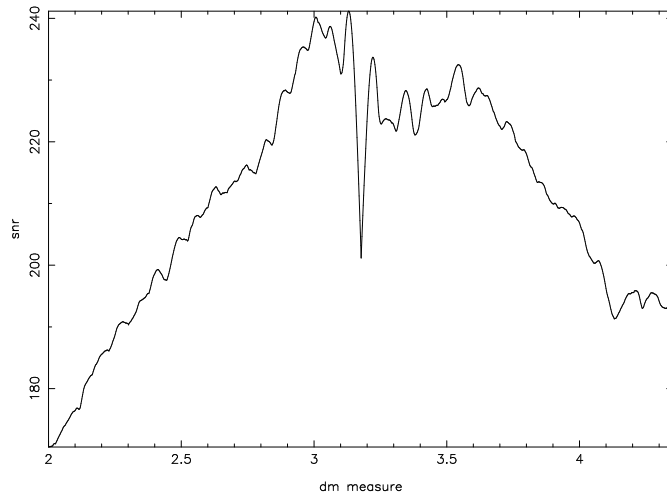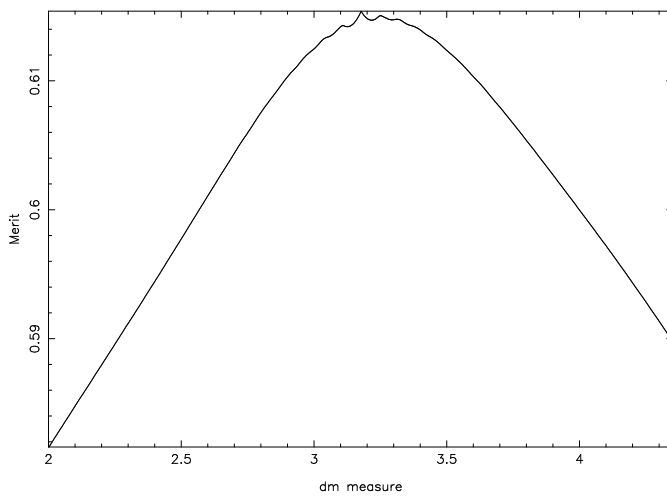
Figure 2.1: SNR as a function of DM

Figure 2.2: Merit as a function of DM

seems to be some systematic enhancement of off-pulse fluctuations occur-ing at some specific delay gradient (i.e. at DM showing dip in SNR).
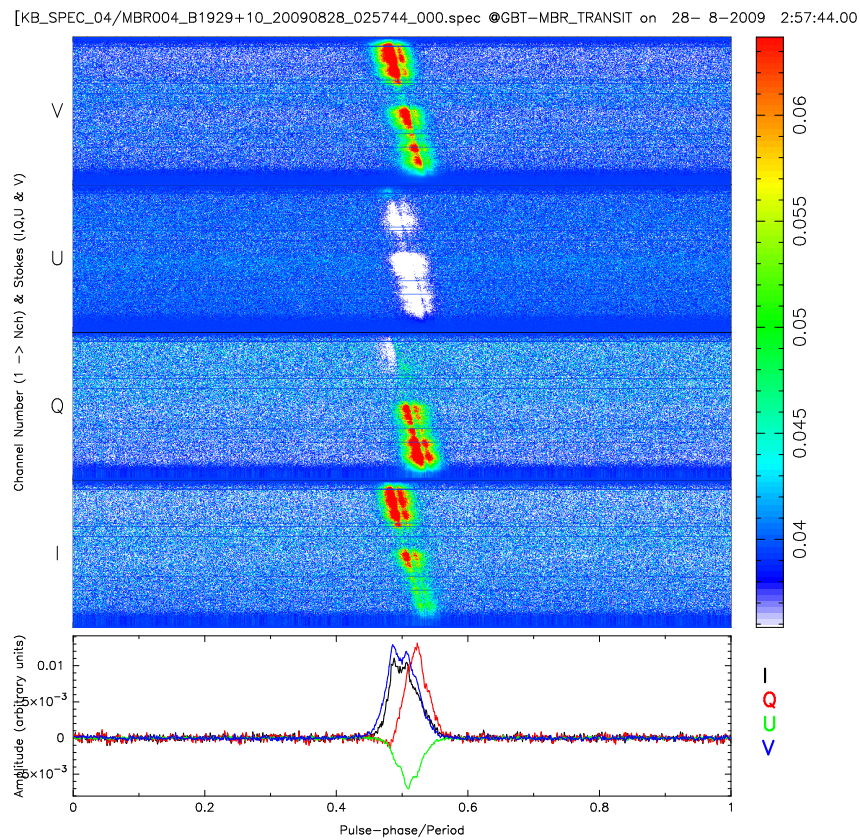

Figure 2.3: 2-d plot of pulse profiles in frequency domain prior to dedis-persion. The sets of profiles across frequency, for each of the Stokes, are stacked together.
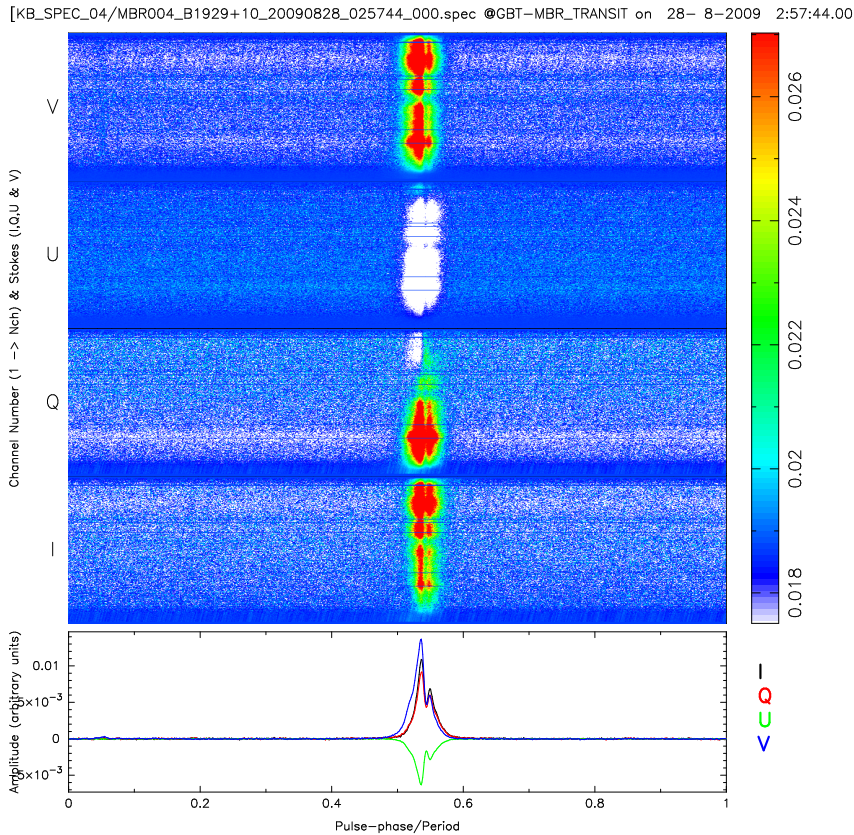
18

Figure 2.4: 2-d plot of pulse profiles in frequency domain after dispersion correction

It is evident from the above plots that after de-dispersion profiles in the different frequency channels align with each other in time (or pulse-phase) domain.

2.1.3 Channel weightage

These aligned profiles in the channels obtained after de-dispersion can be combined further to get an average profile. Since different channel might have different amount of noise, so while combining them, the noisiest channel will worsen the profile quality. Therefore, all the channels are weighed according to their variance (inverse of variance), so that they donâĂŹt adversely affect the profile and neither the information contained in the noisiest channels is lost completely.

For this processing a code has been written such that it takes in the de-

19

dispersed data and then follows the below mentioned steps.

1. Remove the off-pulse mean. The off-pulse mean is estimated by averaging the carefully selected off-pulse bins for all channels.

2. The signal in each channel is normalized by its corresponding on-pulse mean value. The normalization is done so that the pulsar signals in channels do not differ much from each other, and averaging can be done more efficiently.

3. Estimate the variance of noise and corresponding channel weight for each channel. Variance is also estimated over off-pulse bins.

4. Signal in each channel is multiplied with its corresponding channel weight. After combining these channels, an optimally averaged pulse profile is obtained. These weights are decided based on Stokes-I profiles, but applied to all four Stokes when needed.
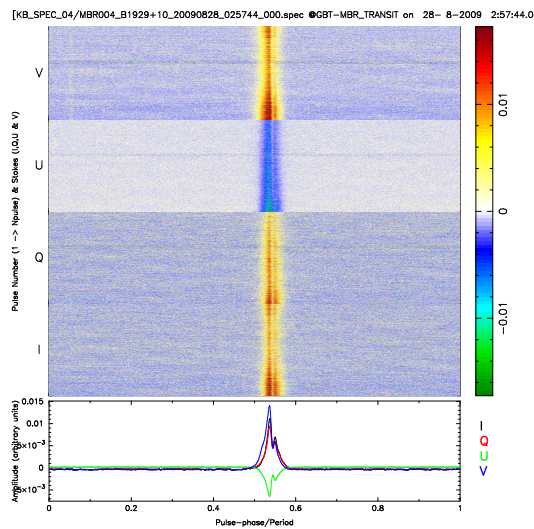
Figure 2.7: 2-d plot of pulse profiles in time domain

Signal-to-noise ratio (SNR) has been obtained by taking the ratio of pulse peak and standard deviation of the noise (in the off-pulse region). Estimated parameters for Band-4, as noted below, illustrate the significant improvement in SNR occuring due to optimal weighting.

SNR of average profile without channel weightage: 92

SNR of average profile with channel weightage: 211

Note that the effective number of channels contributing to the average reduced due to the differential weighting, compared to the total number of spectral channels. The effective number of channels used can be estimated by calculating the ratio of off-pulse mean after processing and raw
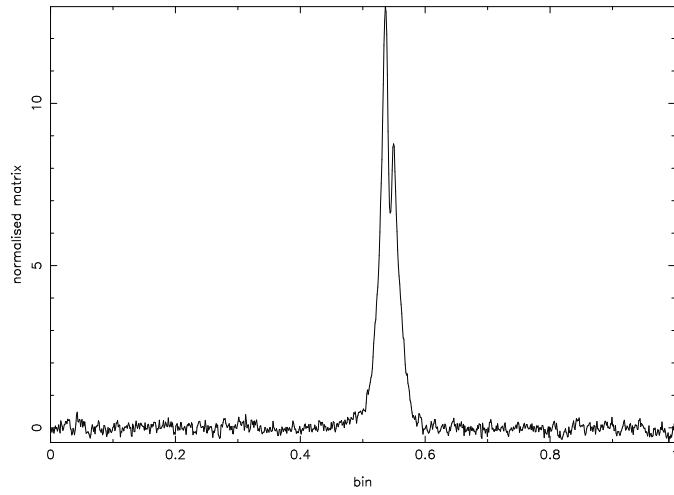
Figure 2.5: Average profile obtained without weighing the channels
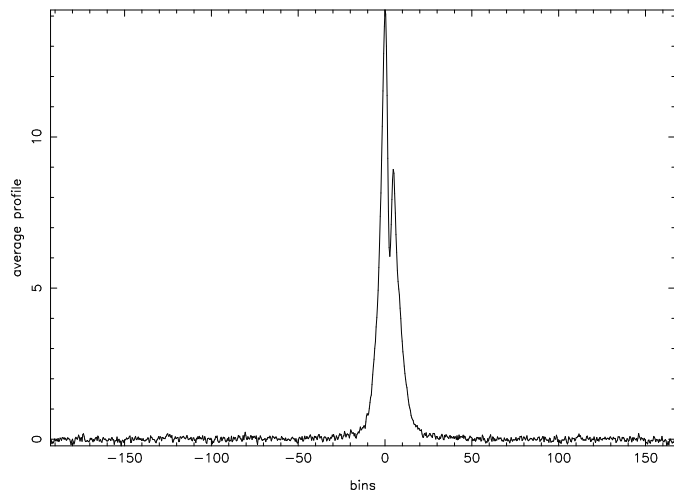
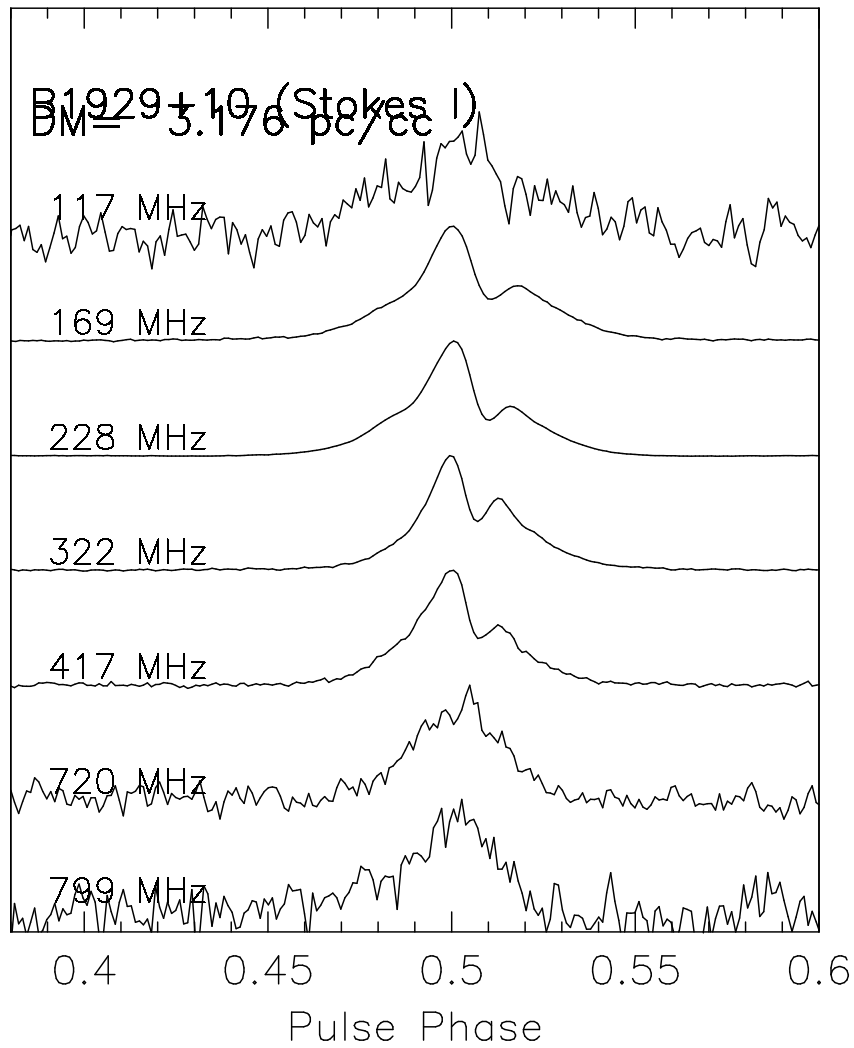Figure 2.6: Average profile obtained after incorporating weightages.

21

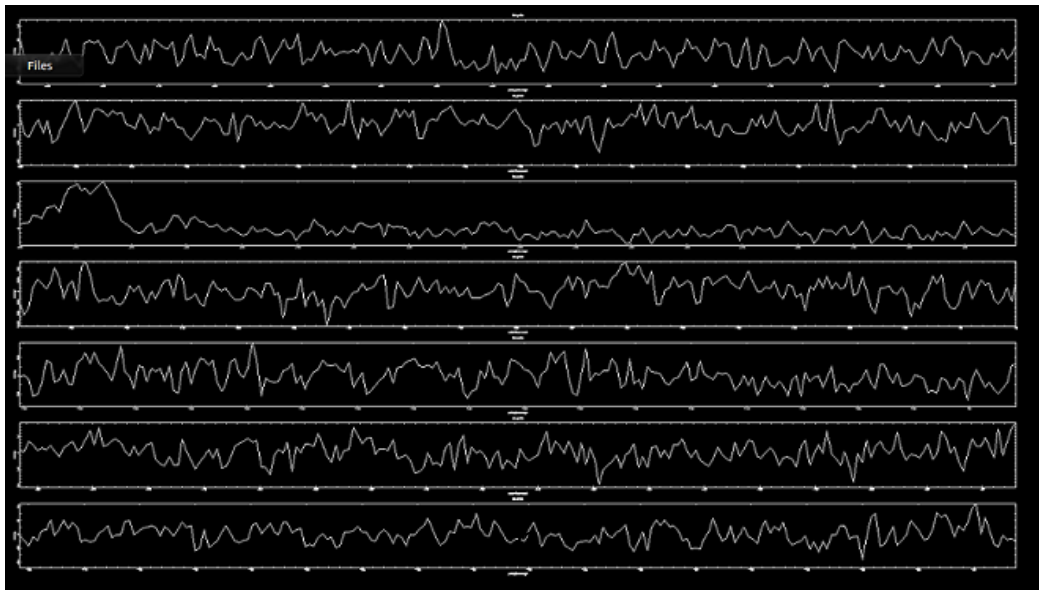Figure 2.8: Aligned Main pulse profiles for all the bands

Figure 2.9: Aligned Inter-pulse profiles for all the bands. The third profile from the top contains an inter-pulse. It occurs in the starting of the profile. Inter-pulse has been seen only in band-3.

off-pulse mean.

2.1.4   Combined average profile

Following the above mentioned procedure, average profiles have been obtained for all other bands as well. Two sets of multi-band aligned profiles have been generated, one for the main-pulse and another for the inter-pulse. These are shown in the following figures.

Structures in the main-pulse The main-pulse contains two components. The separation between the pulse component was studied as a function of frequency. The spectral index -0.3
Component in the pulse represent different emission region.
Inter-pulse was observed only in band-3 due to poor SNR of other bands.
Note: All the above plots and estimated values correspond to Band-4 except the combined (multi-band) plots. Similar calculations have been done for all other bands except band-6,9 and 10 due to poor signal quality in them. Band-3 has highest SNR value but suffers from compression and a strange RFI also has been observed in this band. In the following sections, we discuss these two specific aspects in detail.

2.2   Decompression

2.2.1   Background:

The observed data are in form of time sequences, and successive section of which have been taken to obtain spectral information. Hence, the gain of channels across a given spectrum is same. In presence of strong signal the amplifier gain function, which is mostly linear, enters a mildly non-linear regime (but not in the saturation zone, otherwise there is no escape from certain spectral distortion), and hence, this effect can viewed as the gain changing by only a common factor, due to which compression in the intensity across the spectrum takes place. Even for a mild non-linearity, the effects of compression become apparent.
In the off-pulse region compression does not take place but it does occur in the on-pulse region due to presence of strong pulses. We exploit this fact to correct for this effect. We compare the selected sections of the on-pulse spectrum with the corresponding part of the off-pulse spectrum, treating

the latter as the reference, to determine the factor by which the on-pulse spectrum needs to be corrected. The parts of the on-pulse spectra are selected carefully so that they do not contain pulsar emission.The originally received data which gets affected, is dispersed. Hence, correction values needs to be calculated from the dispersed data.
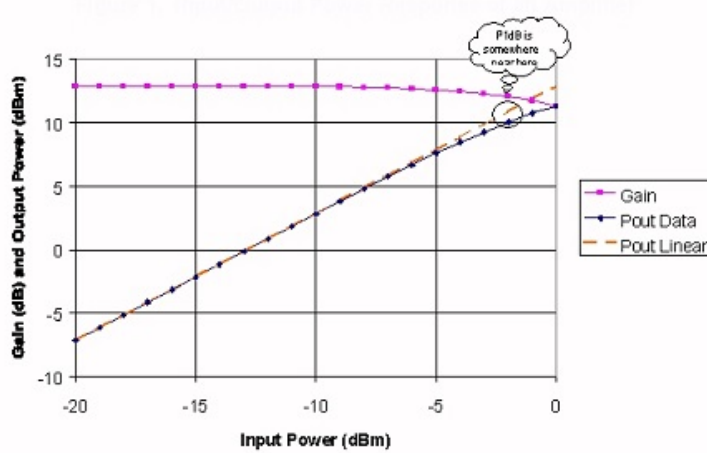

Figure 2.10: Amplifier gain plot where blue curve shows the deviation from linearity.

2.2.2 Simulated Data:

We apply this technique first on the simulated data. This is done to check the applicability of this technique before applying it on the observed pulsar data. A simulated Gaussian pulse which has width same as the pulsar equivalent width is produced. Noise profiles are generated for 256 channels separately. It follows gaussian statistics with different variance (function of channel number) for different channel. On combining the gaussian pulse profile with the noise, we obtain simulated profiles across the frequency channels.
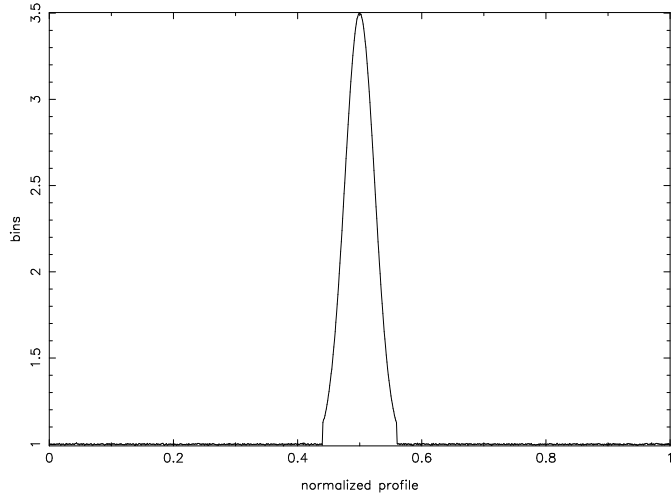
Figure 2.11: Simulated pulse profile
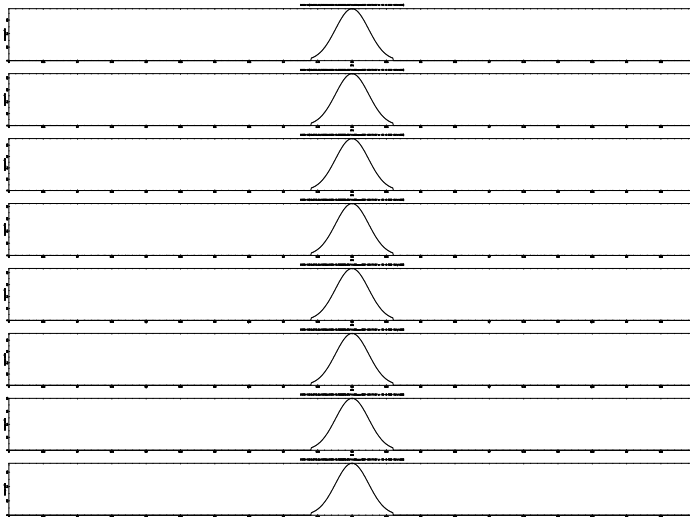
Figure 2.12: Simulated pulse profiles across frequency channels
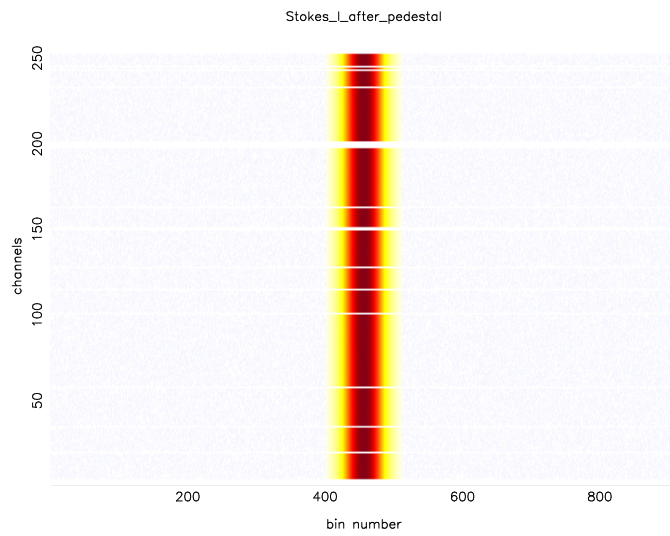
25

Figure 2.13: Simulated profile across frequency channels before dispersion

The above simulated data are modified such that they suffer compression in the on-pulse region. For this purpose, we first disperse the data across the channels, and normalize each channel profile with the corresponding peak value. Gain compression is then applied to these data. Finally, as previously mentioned, we try to obtain the correction factor by comparing the off-pulse spectrum with the selected on-pulse spectrum.
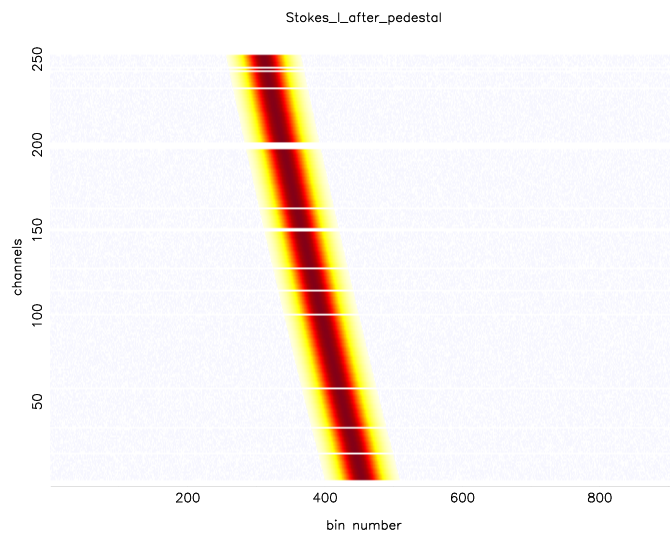
Figure 2.14: Simulated profile across frequency channels after dispersion
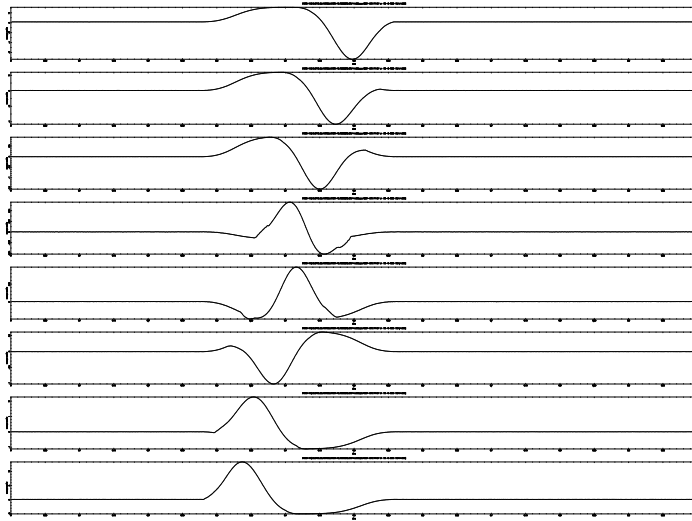
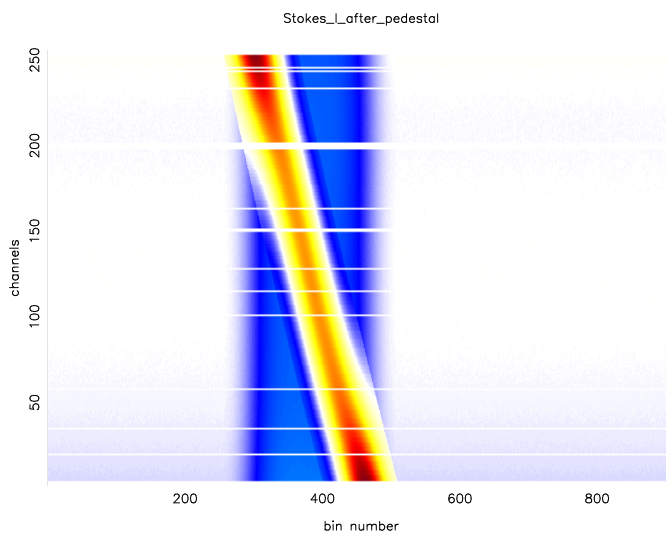Figure 2.15: Dispersed simulated profiles across frequency channels after normalisation.

Figure 2.16: Dispersed simulated profile across frequency channels after normalisation.

Comparision of efficiency of this technique between two cases:
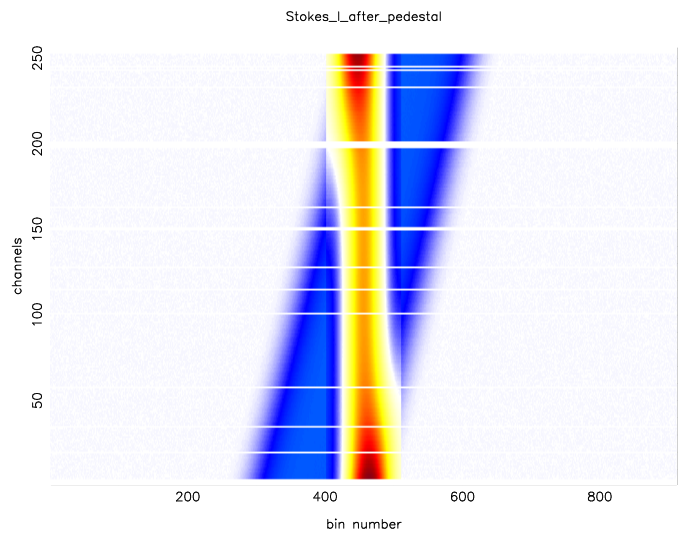1. When DM spread is < pulse width
2. When DM spread is > pulse width

Figure 2.17: Simulated profile before decompression across frequency channels when DM spread is less than pulse width
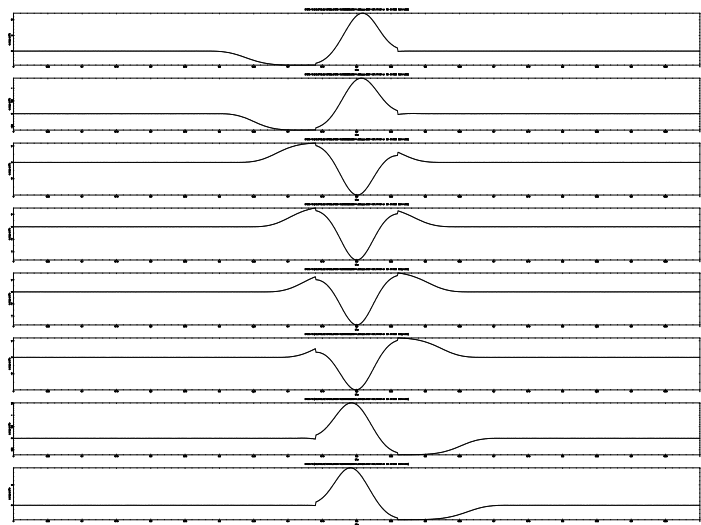

Figure 2.18: Simulated profile before decompression across frequency channels when DM spread is less than pulse width
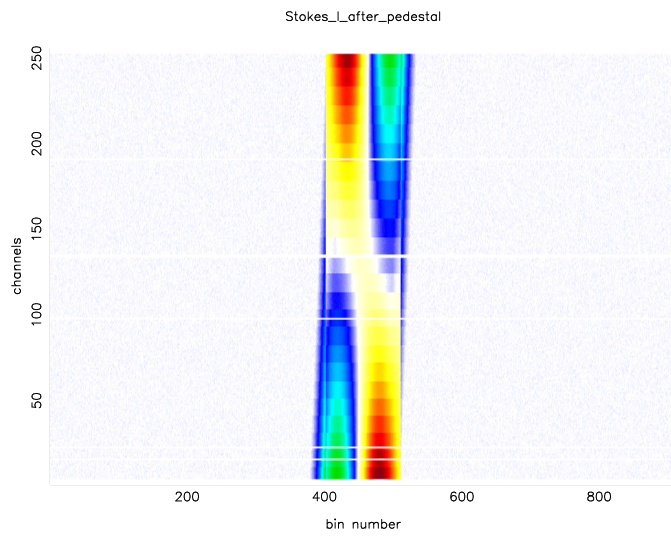
Figure 2.19: Simulated profile before decompression across frequency channels when DM spread is less than pulse width
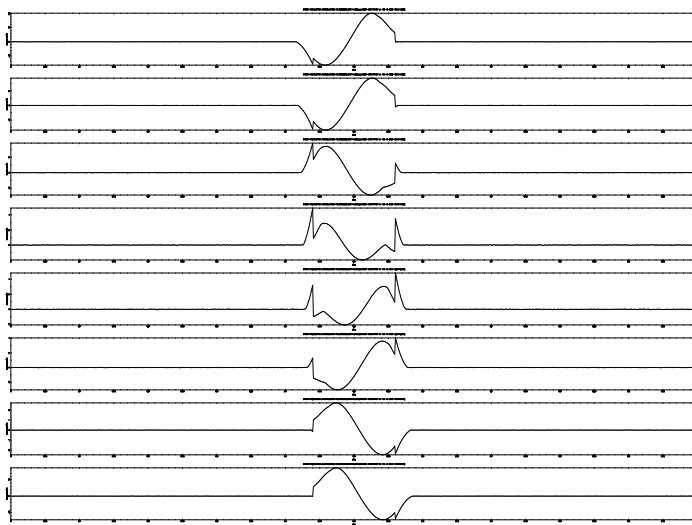

Figure 2.20: Simulated profile before decompression across frequency channels when DM spread is less than pulse width
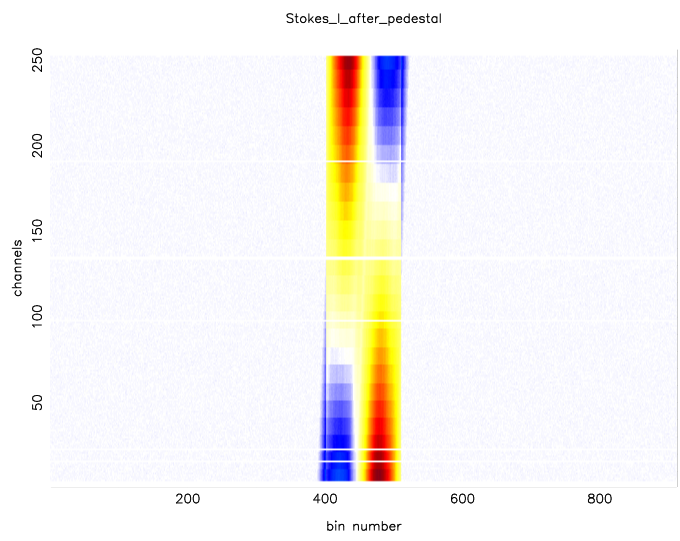
29

Figure 2.21: Simulated profile after decompression across frequency channels when DM spread is less than pulse width
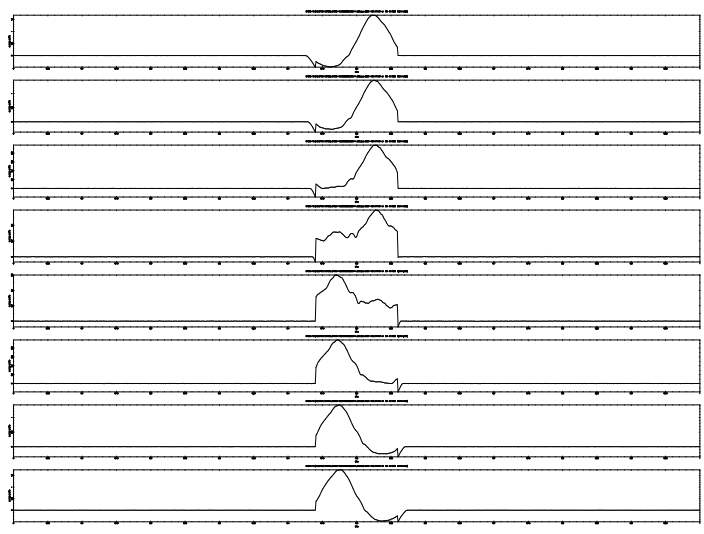

Figure 2.22: Simulated profile after decompression across frequency channels when DM spread is less than pulse width
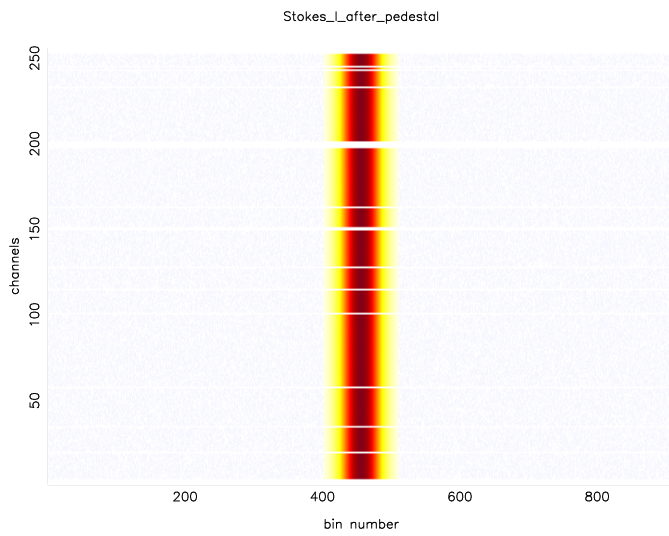
Figure 2.23: Simulated profile after decompression across frequency channels when DM spread is greater than pulse width
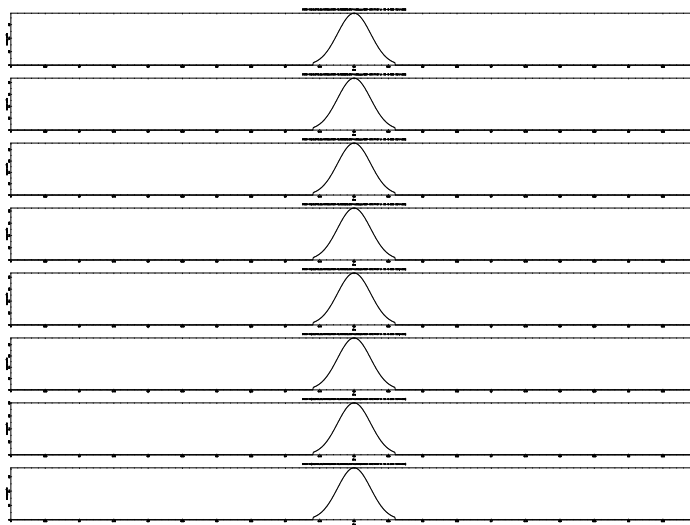

Figure 2.24: Simulated profile after decompression across frequency channels when DM spread is greater than pulse width

In second case, by using this technique compression has been corrected to a very good extent, whereas in first case we still see some compression.

2.2.3   Limitations:

As, we can see from the above analysis that this technique is efficient only when pulse width much narrower than DM spread. The correction factor

31

is obtained from dispersed data. When pulse width is comparable or more than the dispersion width, the number of unaffected becomes very small and hence, it becomes difficult to correct for it. It works better and better when the dispersion delay across a band is much larger than the pulse width.

2.2.4   Observed data:

This effect was observed only in band-3 (Fcen=228MHz). The plots below show the pulse profiles suffered from compression.

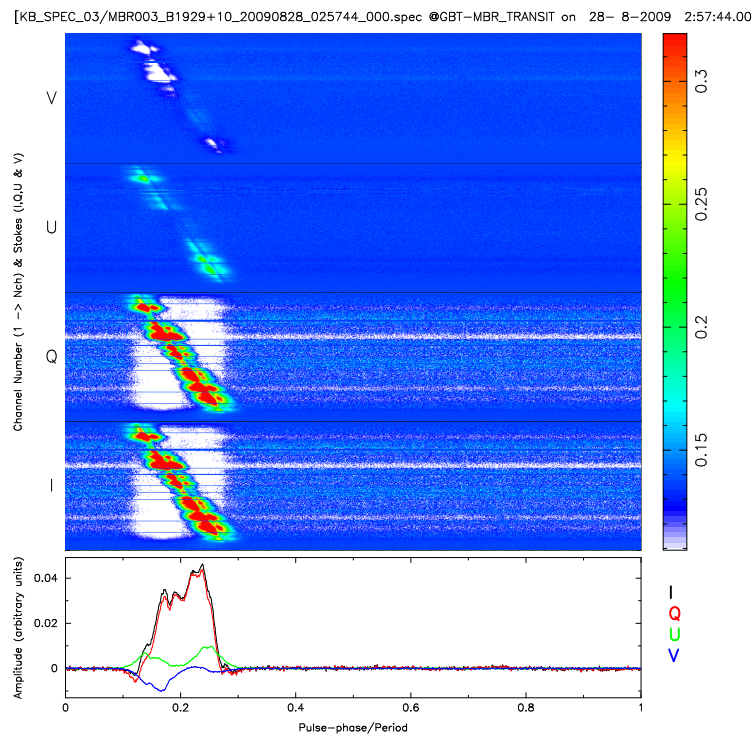Figure 2.25: Dispersed profile of Pulsar B1929+10. The white patches in the off-pulse spectral-region, within the dispersion width are due to compression. These patches are verticle but the pulses are dipersed which implies that this is not a space effect as these are also along frequency channels. These off-pulse spectral region are different from the blue colored off-region as the later one do not suffer from compression.
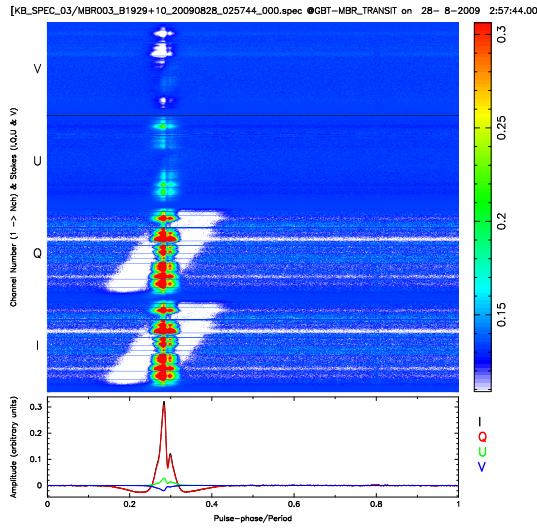
Figure 2.26: De-dispersed profile of Pulsar B1929+10. Here, the white patch has become tilted from verticle due to de-dispersion.
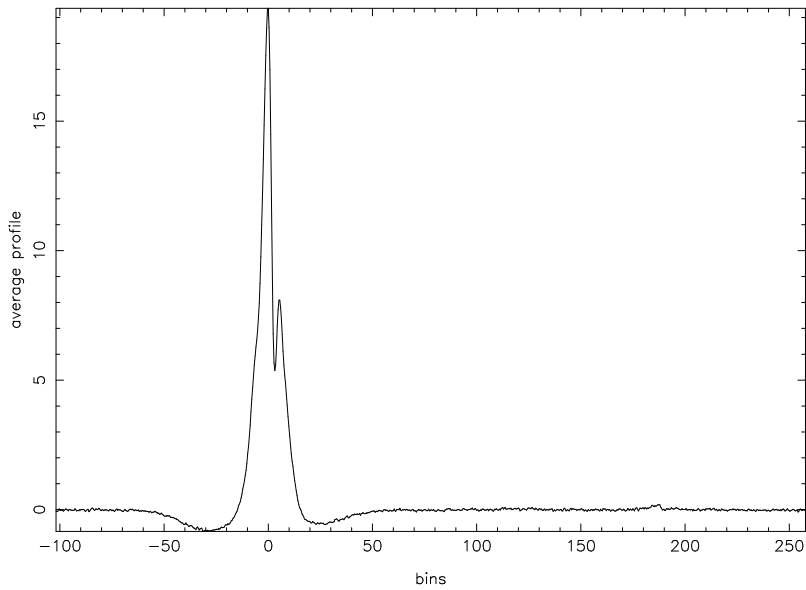

Figure 2.27: Average pulse profile of Pulsar B1929+10 before decompression. The effect of compression is seen on both sides of the main pulse.
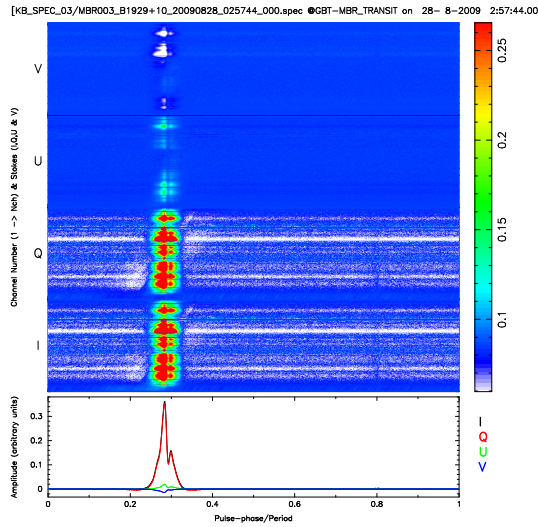
Figure 2.28: De-dipersed profile of Pulsar B1929+10 after decompression. Now, the white patch has almost vanished from the profile implying that the gain is now same across all the bins.
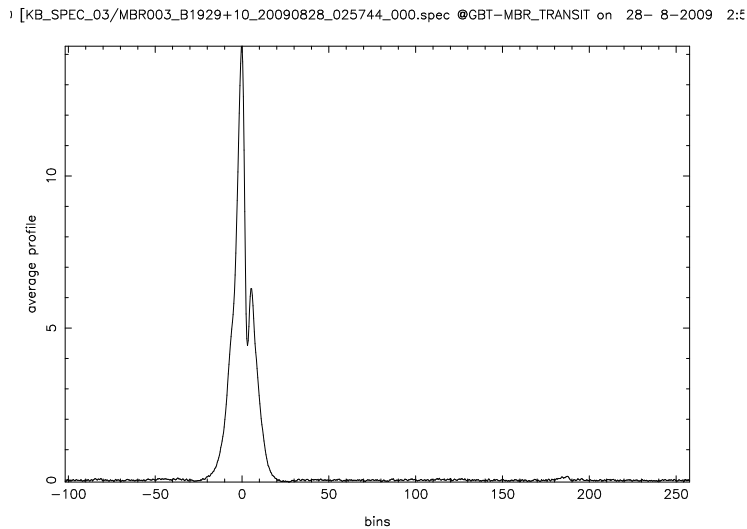
Figure 2.29: Average pulse profile of Pulsar B1929+10 after decompression. There exists an interpulse in this profile at about 190*degree*

At first we had calculated the correction factor from the stokes- I profiles and then used these values to correct for compression, but later we performed decompression separately on Ixx and Iyy, for the following reason. The receiver has two orthogonal polarization receivers. It generates time sequence along X and Y separately. So, instead of stokes-I, Ixx and Iyy are considered separately as they may have different gain values. So

we estimate two sets of correction factors corresponding to Ixx and Iyy separately, using the same procedure/pipeline. First identify the region where pulse in present in both Ixx and Iyy time domain. Once the range has been identified, calculate the flat spectrum. Spectrum will be flat in off-pulse region as this region will not be affected by pulsar signal. For on-pulse region, identify the off-pulse channels and calculate the average area under the curve. The ratio of off-pulse region to on-pulse region area will be the correction factor.

Relative size of pulse minima before decompression in the average profile : 0.035756318

Relative size of pulse minima after decompression in the average profile: 0.004508713

2.3   Strange RFI

While analysing Band-3 (central frequency 228 MHz) a series of harmonics, equally placed at an interval of 18.5 Hz, in the raw data fluctuation spectrum plot was observed. These observed harmonics were different from the harmonics for B1929+10 rotation frequency where the interval between the harmonics is 4.5 Hz. Since the harmonics were periodic, it was important to check if that signal could be from another pulsar or it might just be some terrestrial signal (RFI). So we tried to investigate the reason behind these harmonics.

Procedure:

The time period (inverse of the fundamental frequency) of those pulses was estimated and data was folded for the same period. As the estimated time period was not correct and we could not see any pulse in the signal, so we incorporated search for dispersion measure as well.

DM range to be searched was calculated considering a possibility that the delay caused due to dispersion should be a multiple of its period in order to nullify the entire averaged pulsed signal.

Our observations from these investigations are:

1. Periodic Signal with period = 0.05490781 seconds
2. DM = 0.
3. Though it is periodic but its (reference) phase is not constant for the whole span of observation 20 minutes. From the patches of constant phase it could be seen that it remains constant for some time and then it varies.

35

It changed five times during the observed span.

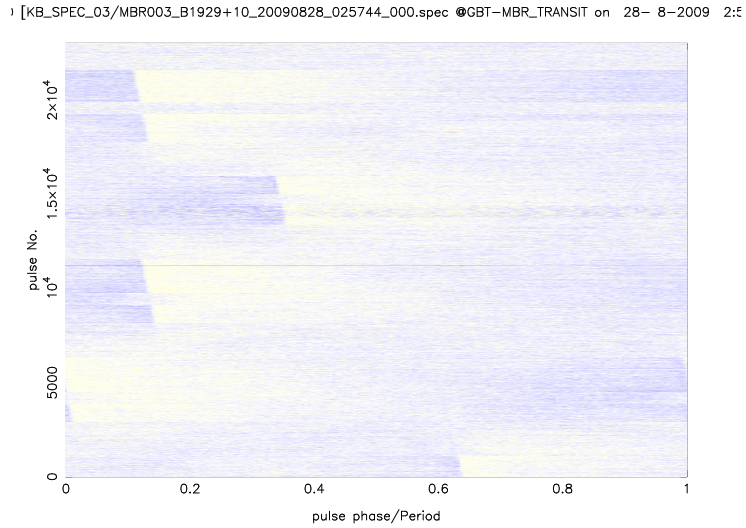
Figure 2.30: RFI pulses placed on top of each other according to their arrival time. These pulses are periodic but they are at different longitude position, implying variation in pulse phase with time.
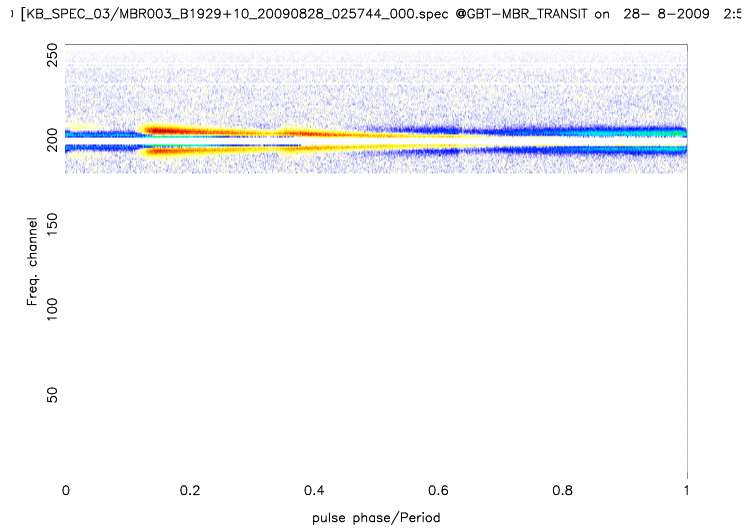
Figure 2.31: A combined plot of RFI pulses in frequency channels. Bright yellow color represents the RFI pulse. It is evident from the plot that these pulses are present only in few channels.
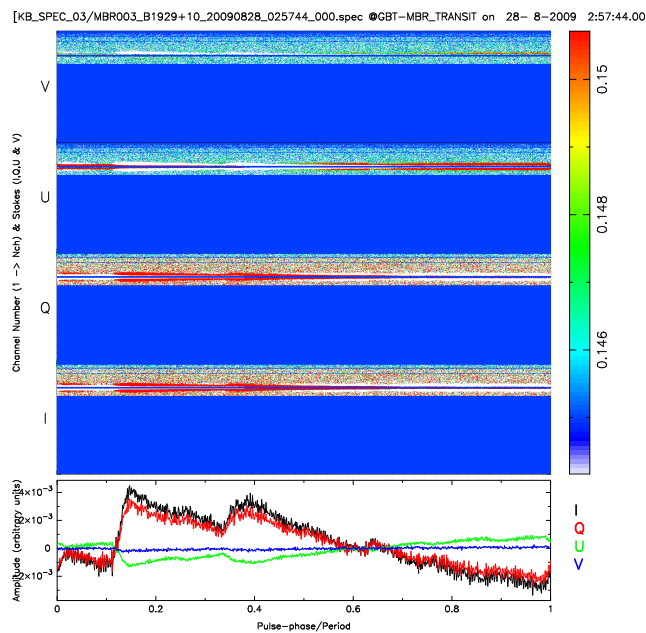
Figure 2.32: Stokes parameter plot of RFI pulses. Non-zero stokes Q and U imply that these pulses are polarized, whereas zero stokes-V intensity implies that there is no circular polarization.
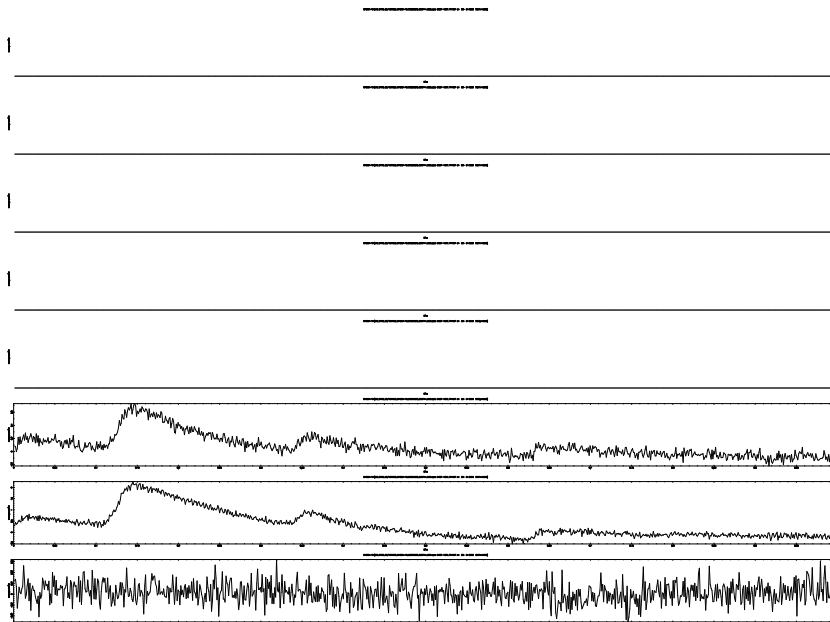
Figure 2.33: This plot shows RFI pulse in various frequency channels.

4. It was confined only to a few channels ranging from channel number

200 to 205. Other channels showed no signature of any such pulse.

5. The pulse has triangular shape and its intensity decreases exponentially along the longitude.
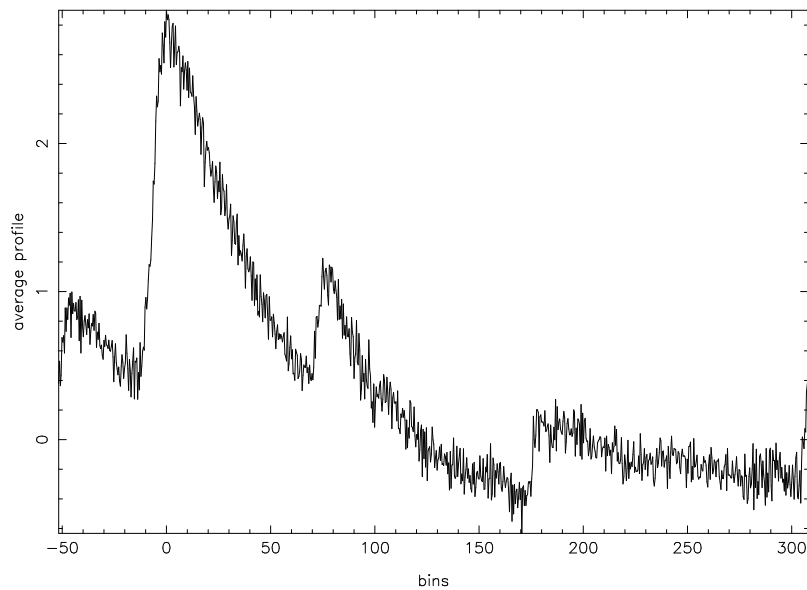
Figure 2.34: Average profile of RFI pulse signal

Conclusions:

DM value = 0 is a very important signature to deduce that it is not an astronomical signal but a terrestrial signal. So, to confirm it further, we looked at the observations of other sources, observed on the same day but at a different time. Harmonics same as these strange harmonics were visible in raw-spectra plots of other sources as well for the same band.
These pulses are strange in a way that the intensity of the signal decreases exponentially and they have non-constant phase. As the strength of this signal is very high, to avoid any interference in further processing these channels has been masked.

2.4 Polarization

2.4.1 What is polarization?

Electromagnetic waves consist of transverse magnetic and electric field. The direction of propagation, magnetic field and electric field are orthogonal to each other. The plane in which the electric field oscillates is defined as the plane of polarization. For example, place a charged particle in presence of EM radiation, the direction in which it oscillates denotes electric field direction and hence, the state of polarization.

Electric field can be represented as combination of two orthogonal polarized waves. The orthogonal components can be given by

$$E_x = \hat{x}\varepsilon_{0x}\cos(kz - \omega t + \Phi_x) \tag{2.7}$$

$$E_y = \hat{y}\varepsilon_{0y}\cos(kz - \omega t + \Phi_y) \tag{2.8}$$

The above equations represent the tip of the electric field vector.

There are three states of polarization: Linear, Circular and Elliptical

Linear: when, $\Phi_x = \Phi_y = \Phi_0$, the x and y component are in phase. Thus, the electric field has constant amplitude and is constrained to oscillate along a fixed direction.

$$E = (\hat{x}\varepsilon_{0x} + \hat{y}\varepsilon_{0y})\cos(kz - \omega t + \Phi_0) \tag{2.9}$$

Circular: when $\varepsilon_{0x} = \varepsilon_{0y} = \varepsilon_0$ and Φ_x - Φ_y = $+-$ $pi/2$

$$E = \varepsilon_0(\hat{x}\cos(kz - \omega t + \Phi_x) - \hat{y}\sin(kz - \omega t + \Phi_y)) \tag{2.10}$$

The direction of electric field varies with time such that its tip traces a circle. If the resultant electric-field rotates in the clockwise direction, it is right circularly polarized. If it is in the reverse direction, it is left circularly polarized.

Elliptical: The elliptical polarization is the most general among the above mentioned states. Linear and circular polarization can be considered as special cases of elliptical polarization. In this case the tip of the electric field trace out an ellipse.

2.4.2 Stokes Parameters

Four stokes parameters I,Q,U and V are defined in order to measure the state of polarization.

$$I = \varepsilon_{0x}^2 + \varepsilon_{0y}^2 = \varepsilon_0^2 \tag{2.11}$$

$$Q = \varepsilon_{0x}^2 - \varepsilon_{0y}^2 \tag{2.12}$$

$$U = \varepsilon_{0x}\varepsilon_{0y}\cos(\Phi_y - \Phi_x) \tag{2.13}$$

$$V = \varepsilon_{0x}\varepsilon_{0y}\sin(\Phi_y - \Phi_x) \tag{2.14}$$

When radiation is fully polarized then

$$I^2 = Q^2 + U^2 + V^2 \tag{2.15}$$

I denotes the total power or intensity of radiation. V denotes circular po-larization as it governs the direction of rotation. V= 0, denotes zero circular polarization. Q and U are used to determine the orientation of linear po-larization.
When
Q = U = V = 0, fully unpolarized radiation.
Q = U = 0, I = V =/ 0 , Purely circular.
V = 0 and remaining parameters non-zero, Purely linear.

If radiation is fully polarized

$$I^2 = Q^2 + U^2 + V^2 \tag{2.16}$$

If radiation is partially polarized

$$I^2 > Q^2 + U^2 + V^2 \tag{2.17}$$

$I^2 - Q^2 + U^2 + V^2$, is unpolarized power.

2.4.3 Faraday Rotation

When a beam of plane polarized light passes through magento-ionic mat-ter such that there exist a component of magnetic field parallel to its di-rection of propagation. It is found that the transmitted light is still plane polarized, but that the plane of polarization is rotated by an angle propor-tional to the magnetic field intensity and square of its wavelength. This *optical* rotation is called the Faraday rotation (or Farady effect).

A plane polarized beam can always be considered as the superposi-tion of two circularly polarized components of the same frequency and of equal amplitude. Different indices of refraction are seen by the left and

right circularly polarized rays, particularly in the magneto-ionic medium. As a result, these rays propagate at different speeds through the medium. When the two rays combine at the end, the resultant ray is plane polarized but offset in the position angle of polarization from the incident ray. Phase rotation can be given by,

$$\theta = RM\lambda^2 \tag{2.18}$$

Where

$$RM = \int_0^D n_e B_{||} * dl \tag{2.19}$$

θ is change in angle due to faraday rotation,
n_e is free electron density of propagation medium in cm$^-$3,
$B_{||}$ is component of magnetic field along the line of sight in μ gauss,
D is distance traversed along the line of sight in parsec(pc),
and λ is the wavelength of radiation.

2.4.4   RM and Position angle estimation

The emission from pulsars is highly polarized. The position angle dictates the orientation of the electric field vector of wave in the plane orthogonal to the direction of wave propagation. The position angle exhibits a S-shaped profile along longitude. The point where maximum change in the polarization angle takes place is known as inflection point. This inflection point does not coincide with main pulse peak. The difference between their position is given by 4r/Rc. Estimation of 'r' helps provides an insight into emission geometry.

The position angle at a particular longitude does not vary with time but due to faraday rotation it varies as a function of frequency. RM can be estimated from the position angle at different frequencies. Suppose there is an antenna which receives linear polarization along only one axis. The power received by the antenna will be maximum when the electric field will be oriented in same direction as of the antenna, and minimum when they are orthogonal. Suppose that the intrinsic position angle is same across the bandwidth but due to Faraday rotation signals different channels will have different phase angle([13]). Hence, power received will be a function of frequency.

Assume that the electric field makes an angle of θ with the antenna. Power received by the antenna can be given by

$$P = (E_0 * cos(\theta))^2 \tag{2.20}$$

Apparent position angle can be given as:

$$\theta = \theta_0 + RM * \lambda^2 \tag{2.21}$$

Power received by the antenna is a function of both intrinsic position angle and the radition wavelength.

$$P = E_0^2/2 + (E_0^2/2)\cos(2(\theta_0 + RM\lambda^2)) \tag{2.22}$$

Non-linear least square fitting has been used to model and extract the RM value. This technique exploits the fact that sine and cosine are orthogonal functions. For a range of RM values, template spectras and basis functions are calculated. Then these spectras are cross correlated with different basis function. Ideally, cross-correlation will be zero except for the correct RM value and hence, a maximum will exist at that point.

$$P = P_0 + P_0\cos(\theta_1)cos(\theta_0) - P_0\,sin(\theta_1)\sin(\theta_0) \tag{2.23}$$

1, $\cos(\theta_1)$,and $\sin(\theta_1)$ can be considered as basis functions and, $\cos(\theta_0)$ and $\sin(\theta_0)$ correcponding coefficients.

Following steps need to be followed to determine RM.

1. Take a range of RM value.
2. Calculate basis function for each channel for each RM value.
Position angle at a particular RM and frequency is given by,

$$\theta_1(RM_i, chn_j) = RM * (c^2) * (1/f_1^2 - 1/f_j^2) \tag{2.24}$$

3. Remove the mean spectral power from the spectra.
4. Multiply the residual spectra with basis functions for different RM values and then average it over all the channels.
5. Study the variation in spectral intensity at one longitude angle as a function of RM. The RM at which maximum occurs corresponds to the RM of pulsar.
Polarization position angle estimation:
The ratio of components corresponding to basis functions for estimated RM value, gives the phase angle.

$$PA = (1/2)\tan^{-1}(\sin(\theta_0)/cos(\theta_0)) \tag{2.25}$$

2.4.5 PA estimation for simulated Data

We have simulated data such that it has only linear polarization, there is no circular polarization. Two orthogonally polarized field vectors Ex and Ey has been generated. These are given by,

$$E_x = E_1(\phi)B(\mu)\cos(\alpha) \tag{2.26}$$

$$E_y = E_2(\phi)B(\mu)\sin(\alpha) \tag{2.27}$$

Where, E_1 and E_2 are gaussian pulses as a function of longitude, with different amplitudes,
B is bandshape function,
α is phase angle which contains intrinsic position angle and also, the orientation change due to faraday rotation,
ϕ is longitude phase, and μ is frequency.
Stokes I, Q, U and V are obtained from Ex and Ey using the above stokes equations.
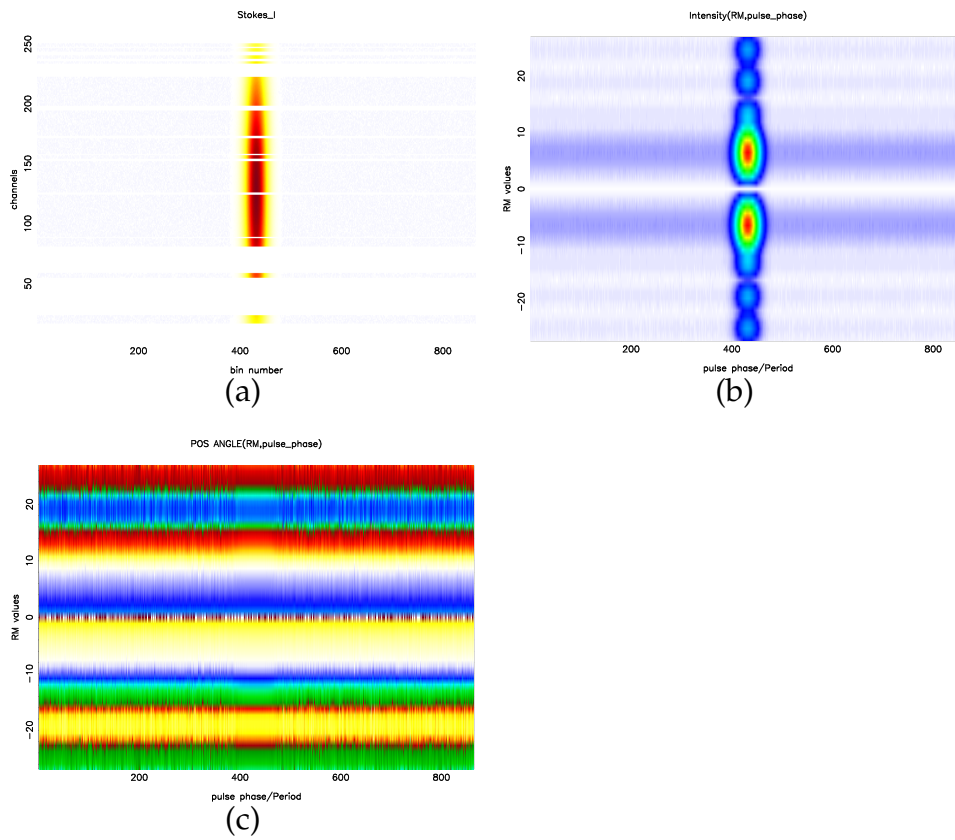
(a)

(b)

(c)

Figure 2.35: (a) Simulated stokes I intensity profile. (b) Fourier transformed stokes-I in RM domain (c) PA profile of simulated I for a range of RM values. Since the bandshape effect has not been removed there is modulation in stokes I.
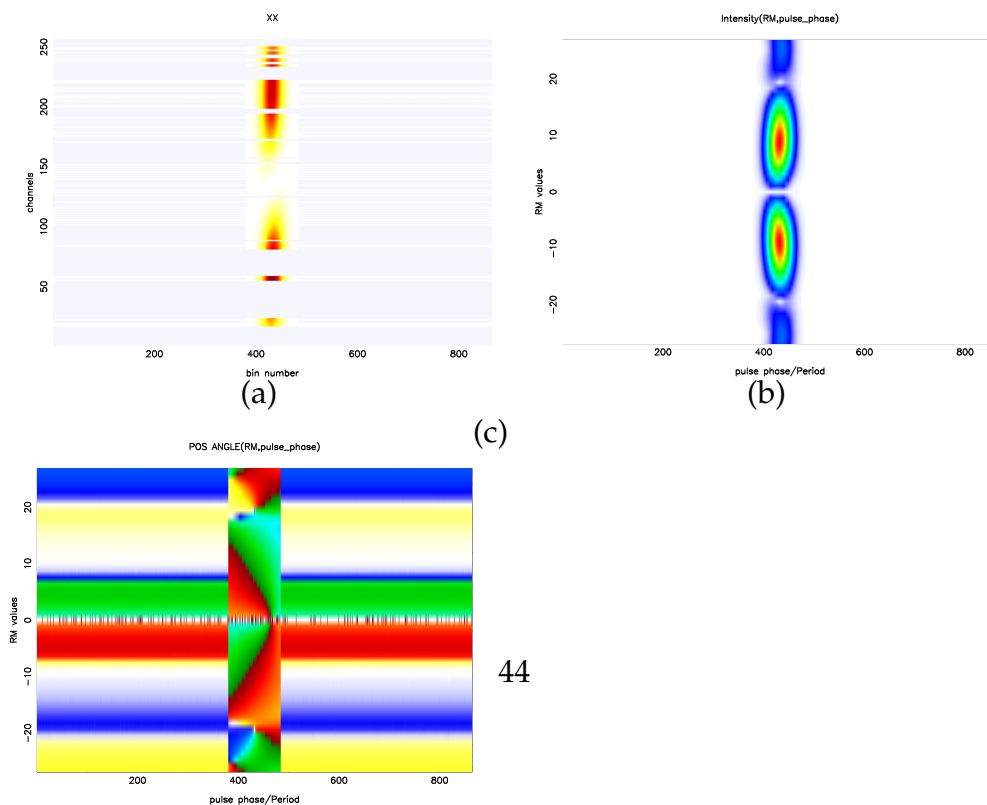

(a)

(b)

(c)

44

Figure 2.36: (a) Simulated Ixx intensity profile. (b) Fourier transformed Ixx in RM domain (c) PA profile of simulated Ixx for a range of RM values
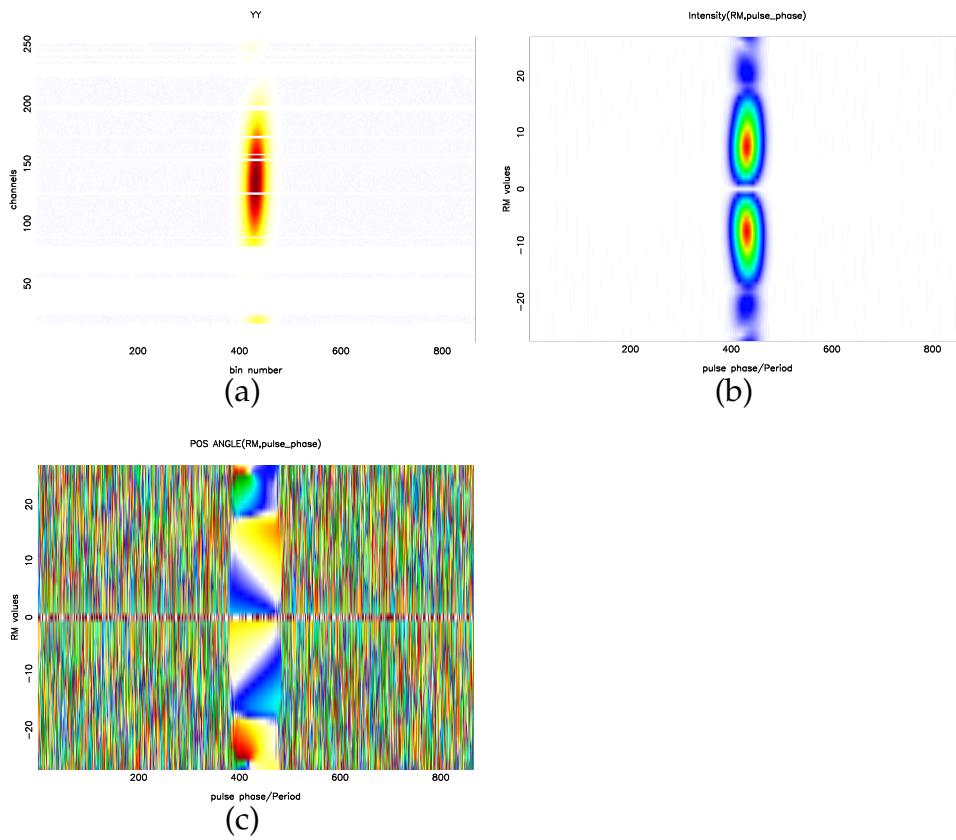
Figure 2.37: (a) Simulated Iyy intensity profile (b)Fourier transformed Iyy in RM domain (c) PA profile of simulated Iyy for a range of RM values
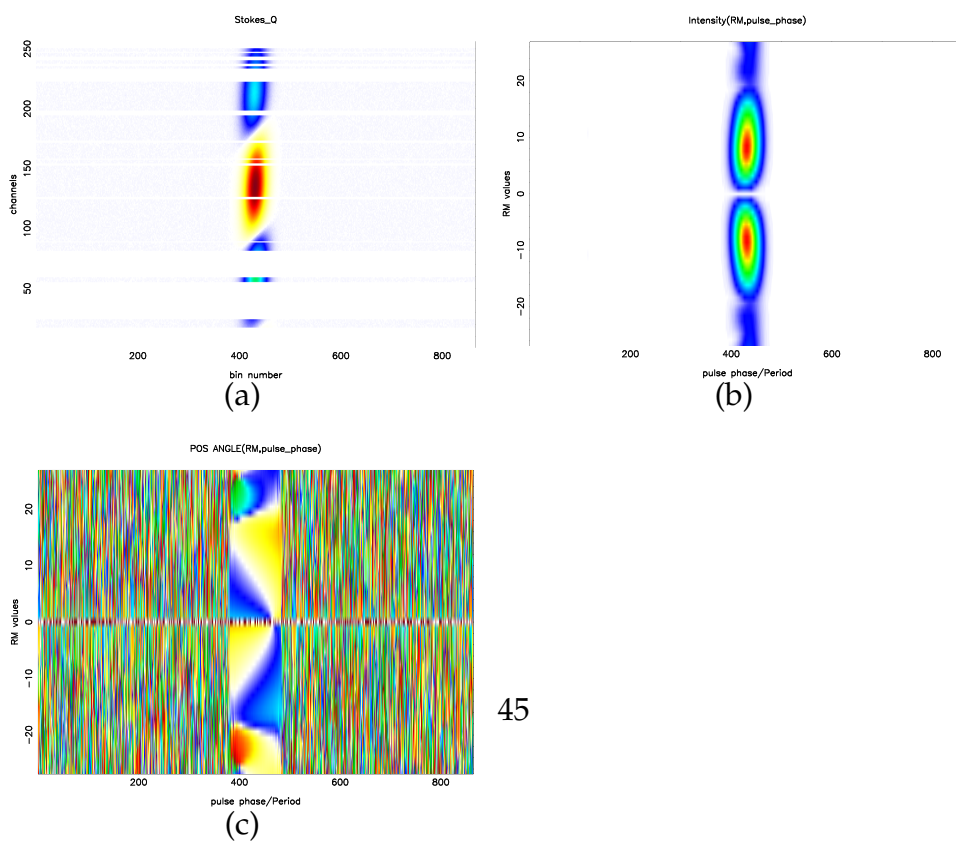

45

Figure 2.38: (a) Simulated stokes Q intensity profile (b) Fourier transformed stokes-Q in RM domain (c) PA profile of simulated Q for a range of RM values
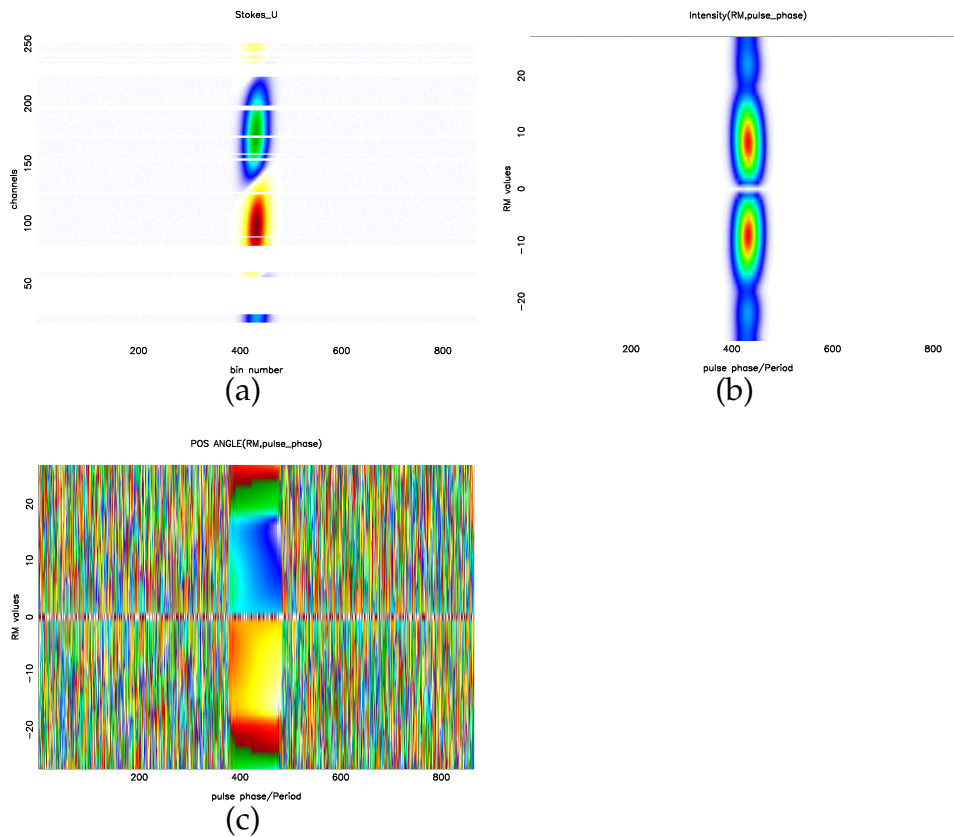
Figure 2.39: (a) Simulated stokes U intensity profile (b) Fourier transformed stokes-U in RM domain (c) PA profile of simulated U for a range of RM values

2.4.6 Observed Data

Although our data have full polarization information through use of dual orthogonal polarisation channels and their cross correlations, we have first looked at each channel separately for possible spectral modulation resulting from frequency dependent Faraday rotation. Here, we have computed position angle profile corresponding to Ixx and Iyy separately. PA angle information is same in both Ixx and Iyy except the sign of RM value.
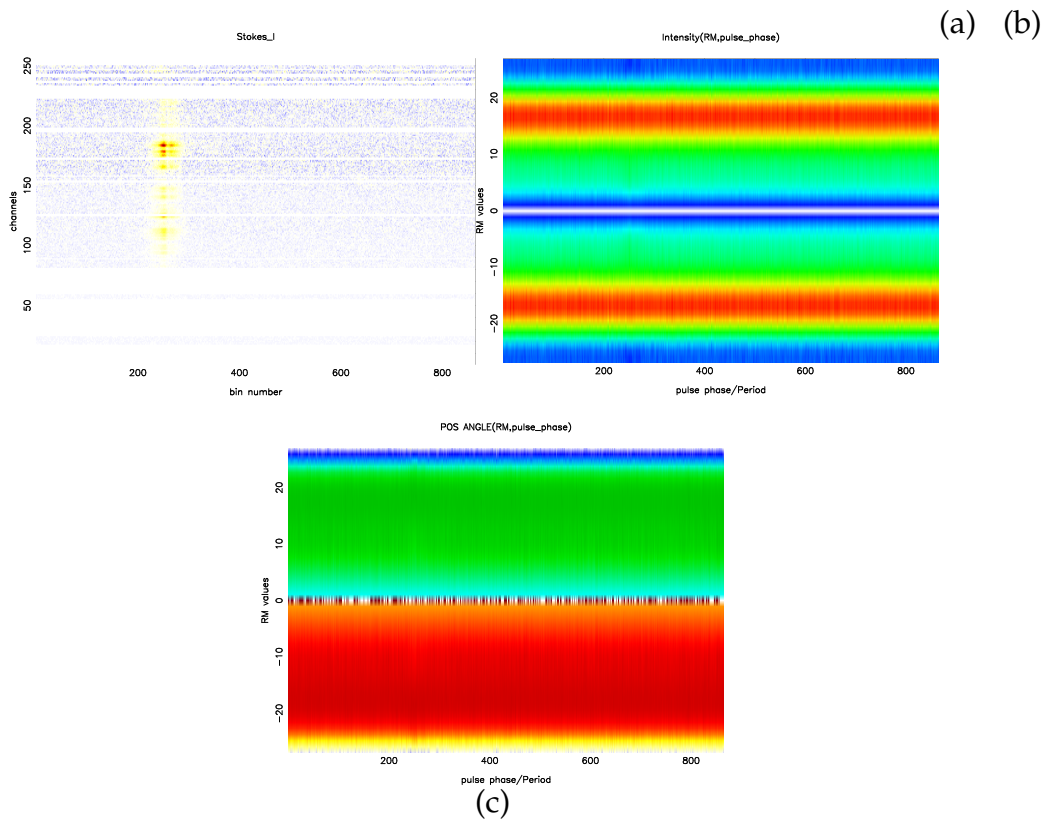
Figure 2.40: (a) Stokes I intensity profile (b) Fourier transformed stokes-I in RM domain (c) PA profile of I for a range of RM values
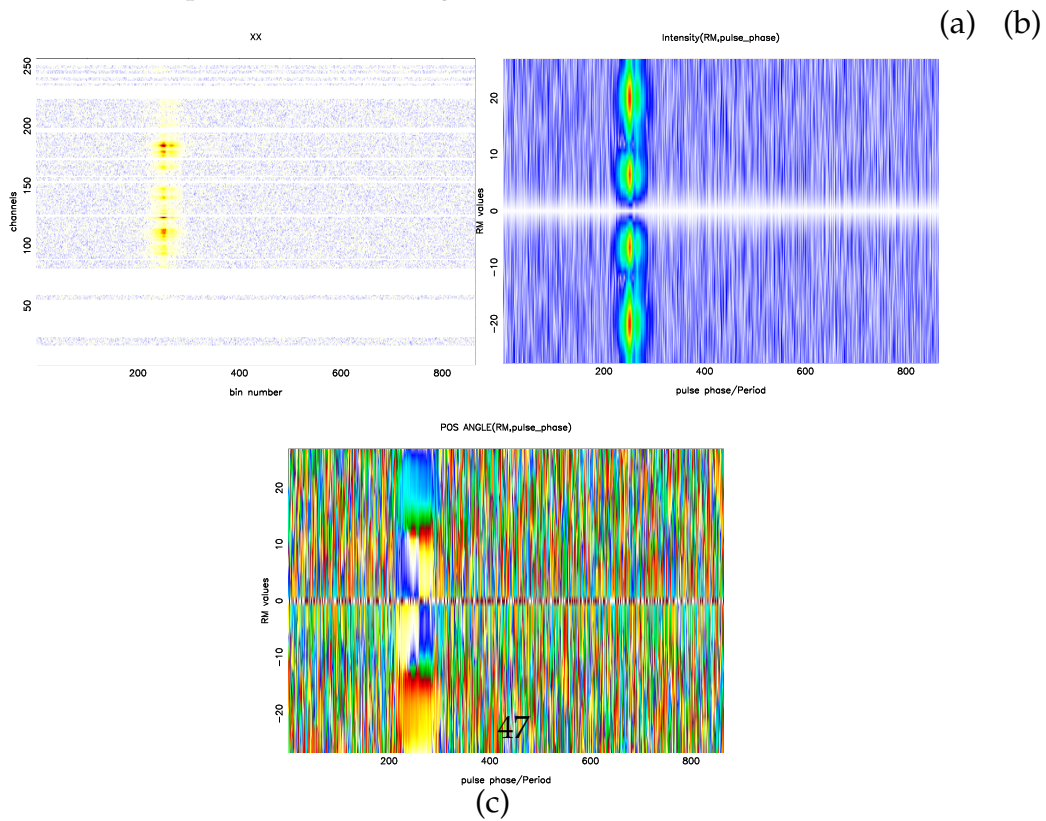

47

Figure 2.41: (a) Ixx intensity profile (b) Fourier transformed Ixx in RM domain (c) PA profile of Ixx for a range of RM values
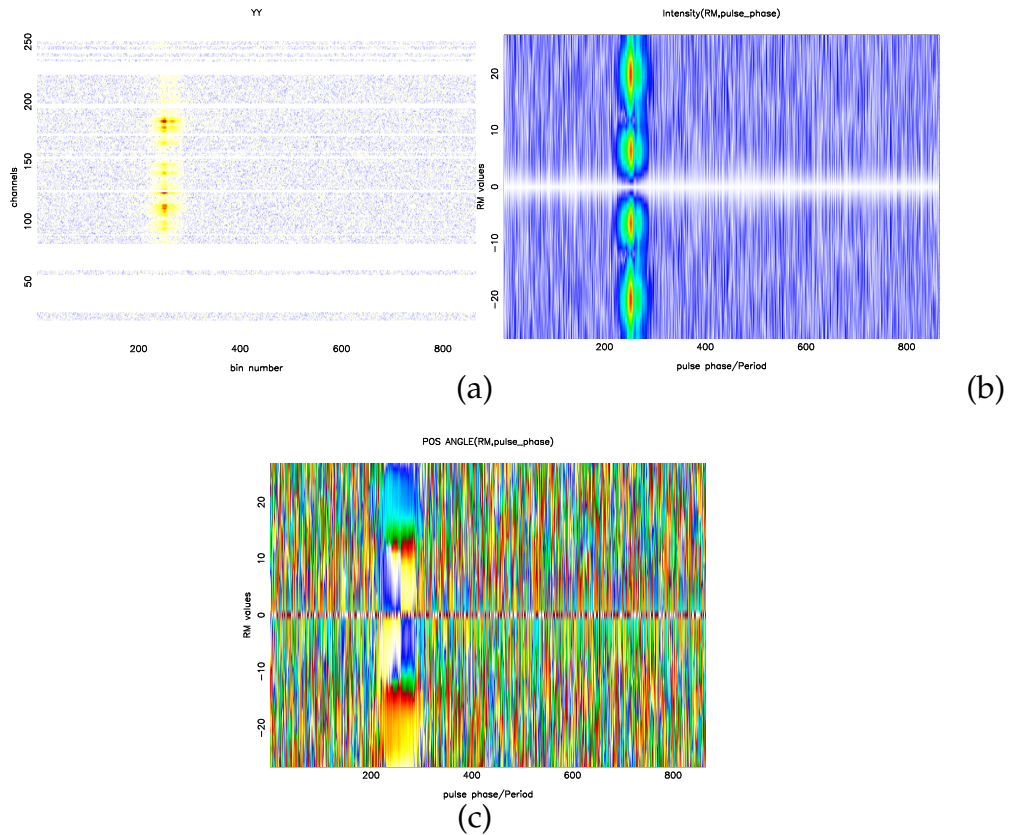
Figure 2.42: (a)Iyy intensity profile (b)Fourier transformed Iyy in RM domain (c)PA profile of Iyy for a range of RM values

As, we have not removed the bandshape from the data,its effect can be seen in form of modulation in all the stokes plots. We plan to correct for the bandshape so that the reason behind stokes-I modulation becomes apparent.

Limitations:

RM value should be large enough to have atleast one modulation cycle across the bandwidth. This technique is limited by the bandwidth, number of channels and central frequency. As, for higher frequency the phase change will be small and hence, small modulation which would require large bandwidth. When the number of channels is large, the chanel bandwidth becomes broad and if RM value is large such that more than modulation cycle occur within a channel then we wont be able to account for it. Thus, there is always uncertainity in the estimated RM value.

Chapter 3

Conclusion

3.1 So far.....

We obtained average pulse profiles for all the bands, except Band-6,9 and 10 due to the poor to quality of signal in them. The intensity of pulsar signal was maximum in Band-3 (227 MHz), after that it falls on either side on frequency bands.

The maximum SNR that we could achieve was 800, but in order to study notches we need SNR 6000. Hence, unfortunately notches could not be studied.

We estimated several other quantities those related to pulsar and also, those related to instrument/analysis. These are listed below:

1. Effective number of channels used as result of weighted average(for eg in band-4 it was 82.05%.

2. Artifact due to compression cause dips in the pulse intensity on the either side of the maxima and decompression correction removes this artifact. for example the dip before correcation on the negative side was 3.5% . The correction presented in removing the dip with intensity, now within 0.5% of above zero. Indicating the significance of this correction. Simulation of the compression effect showed that decompression is effective only when pulse width is less than the dispersion width.

3.The distance between the main pulse components was estimated at each frequency in each band and was found to be decreasing with increasing frequency. The estimated spectral index of this variation is -0.357052 (Âś0.05561). This is consistent with the expected value from the Ruderman Sutherland theory and steeper than what Rankin had observed in one of the pulsars.

4. Faraday rotation induced modulation in the spectra of Ixx and Iyy were examined and related position angle profile as a function of pulse longiude were estimated. both of them showed variation of position angle across longitude consistent with the profile seen by rankin, including a wiggle feature in the PA traverse.

However, the immense similarity between Ixx and Iyy PA profile is wholesome. Since, we had expected them to show have PA difference of $90°$. The observed similarity suggests a common source of modulation between the polarization channels.

Modulation in stokes I has indeed been seen similar to above and is most likely due to inter-stellar scintillation which needs to be corrected for before the faraday rotation induced modulation becomes visible. This correction needs to be done and also carefully.

3.2   Further investigations:

1. Altitude dependent polarization:
The profile centre and inflection point in the PA profile are not expected to be same. The profile centre is expected to lag the inflection point by 4r/Rc([12]). This delay is not due to aberration or time delay effect but due to rotational effects, as the trajectories of electrons are bent forward in inertial frame of the reference with respect to corotation frame. The above factor can be used to estimate the location (altitude) of emission.
2. Presence of Notches:
We aim revisit and possibly optimize the pulse folding for band-3 to see if we can detect notches. Study of variation of spacing between the notches and MP as a function of frequency would then be possible.
3. We also plan to look at pulse to pulse fluctuation and possible perioidicity in the fluctuation spectrum.

References

[1] J. M. Rankin, Toward an empirical theory of pulsar emission. I Morphological taxonomy., 274 (1983) 333–368. doi:10.1086/161450 .

[2] V. Radhakrishnan, D. J. Cooke, Magnetic Poles and the Polarization Structure of Pulsar Radiation, 3 (1969) 225.

[3] P. Goldreich, W. H. Julian, Pulsar Electrodynamics, 157 (1969) 869. doi:10.1086/150119 .

[4] M. A. Ruderman, P. G. Sutherland, Theory of pulsars - Polar caps, sparks, and coherent microwave radiation, 196 (1975) 51–72. doi:10.1086/153393 .

[5] J. M. Rankin, N. Rathnasree, On the Polarisation and Emission Geometry of Pulsar 1929+10: Does Its Emission Come from a Single Pole or Two Poles?, Journal of Astrophysics and Astronomy 18 (1997) 91. doi:10.1007/BF02714873 .

[6] J. Navarro, R. N. Manchester, J. S. Sandhu, S. R. Kulkarni, M. Bailes, Mean Pulse Shape and Polarization of PSR J0437-4715, 486 (1997) 1019. doi:10.1086/304563 .

[7] M. A. McLaughlin, J. M. Rankin, 'Notches' in the average profiles of bright pulsars, 351 (2004) 808–812. arXiv:astro-ph/0311498 , doi:10.1111/j.1365-2966.2004.07937.x .

[8] J. Dyks, Altitude-dependent polarization in radio pulsars, 391 (2008) 859–868. arXiv:0806.0554 , doi:10.1111/j.1365-2966.2008.13923.x .

[9] J. Dyks, B. Rudak, P. Demorest, The nature of pulsar radio emission, 401 (2010) 1781–1795. arXiv:0908.1359 , doi:10.1111/j.1365-2966.2009.15679.x .

[10] G. A. E. Wright, A model for 'double notches' in radio pulsar profiles, 351 (2004) 813–822. `arXiv:astro-ph/0311467`, `doi:10.1111/j.1365-2966.2004.07729.x`.

[11] J. Dyks, B. Rudak, J. M. Rankin, A model for double notches and bifurcated components in radio profiles of pulsars and magnetars. Evidence for the parallel acceleration maser in pulsar magnetosphere, 465 (2007) 981–991. `arXiv:astro-ph/0610883`, `doi:10.1051/0004-6361:20066657`.

[12] Y. Maan, A. A. Deshpande, V. Chandrashekar, J. Chennamangalam, K. B. Raghavendra Rao, R. Somashekar, G. Anderson, M. S. Ezhilarasi, S. Sujatha, S. Kasturi, P. Sandhya, J. Bauserman, R. Duraichelvan, S. Amiri, H. A. Aswathappa, I. V. Barve, G. Sarabagopalan, H. M. Ananda, C. Beaudet, M. Bloss, D. B. Dhamnekar, D. Egan, J. Ford, S. Krishnamurthy, N. Mehta, A. H. Minter, H. N. Nagaraja, M. Narayanaswamy, K. O'Neil, W. Raja, H. Sahasrabudhe, A. Shelton, K. S. Srivani, H. V. Venugopal, S. T. Viswanathan, RRI-GBT Multiband Receiver: Motivation, Design, and Development, 204 (2013) 12. `arXiv:1210.2573`, `doi:10.1088/0067-0049/204/1/12`.

[13] A. A. Deshpande, R. Ramachandran, V. Radhakrishnan, The observational evidence pertinent to possible kick mechanisms in neutron stars, 351 (1999) 195–200. `arXiv:astro-ph/9910103`.

[14] A. G. Lyne, R. N. Manchester, The shape of pulsar radio beams, 234 (1988) 477–508.

[15] J. Dyks, M. Frąckowiak, A. Słowikowska, B. Rudak, B. Zhang, The Pulsar Shadow as the Origin of Double Notches in Radio Pulse Profiles, 633 (2005) 1101–1113. `arXiv:astro-ph/0503411`, `doi:10.1086/466508`.

[16] F. Michel, Theory of Pulsar Magnetospheres, Reprint ... from Reviews of modern physics, American Physical Society, 1982.
URL `http://books.google.co.in/books?id=f2fzHAAACAAJ`

[17] D. Lorimer, Handbook of Pulsar Astronomy, Cambridge Observing Handbooks for Research Astronomers, Cambridge University Press, 2005.
URL `http://books.google.co.in/books?id=OZ8tdN6qJcsC`

[18] G. Rybicki, A. Lightman, Radiative Processes in Astrophysics, Physics textbook, Wiley, 2008.
URL http://books.google.co.in/books?id=eswe2StAspsC

Certificate

This is to certify that this thesis entitled *"Multi-Frequency Study of Pulsar B1929+10"* submitted towards the partial fulfilment of the BS-MS dual degree programme at the Indian Institute of Science Education and Research Pune represents original research carried out by **Karishma Bansal** at the Raman Research Institute, Bengaluru under the supervision of **Avinash Deshpande** during the academic year 2013-2014.

Karishma Bansal
20091108

Avinash Deshpande
Professor, RRI Bengaluru